Human Molecular Genetics, 2014, Vol. 23, No. 16 **4215–4231**
doi:10.1093/hmg/ddu140
Advance Access published on April 4, 2014

Tbx1 is required autonomously for cell survival and fate in the pharyngeal core mesoderm to form the muscles of mastication

Ping Kong[1,†], Silvia E. Racedo[1,†], Stephania Macchiarulo[1], Zunju Hu[1], Courtney Carpenter[2], Tingwei Guo[1], Tao Wang[3], Deyou Zheng[1,4] and Bernice E. Morrow[1,*]

[1]Department of Genetics, Albert Einstein College of Medicine, 1301 Morris Park Avenue, Bronx, NY 10461, USA, [2]Department of Surgery, Montefiore Medical Center, 111 East 210th Street, Bronx, NY 10467, USA, [3]Department of Epidemiology and Population Health, Department of Genetics, Albert Einstein College of Medicine, 1300 Morris Park Avenue, Bronx, NY 10461, USA and [4]Departments of Neurology and Neuroscience, Department of Genetics, Albert Einstein College of Medicine, 1300 Morris Park Avenue, Bronx, NY 10461, USA

Received October 17, 2013; Revised February 21, 2014; Accepted March 24, 2014

Velo-cardio-facial/DiGeorge syndrome, also known as 22q11.2 deletion syndrome, is a congenital anomaly disorder characterized by craniofacial anomalies including velo-pharyngeal insufficiency, facial muscle hypotonia and feeding difficulties, in part due to hypoplasia of the branchiomeric muscles. Inactivation of both alleles of mouse *Tbx1*, encoding a T-box transcription factor, deleted on chromosome 22q11.2, results in reduction or loss of branchiomeric muscles. To identify downstream pathways, we performed gene profiling of microdissected pharyngeal arch one (PA1) from *Tbx1*$^{+/+}$ and *Tbx1*$^{-/-}$ embryos at stages E9.5 (somites 20–25) and E10.5 (somites 30–35). Basic helix–loop–helix (bHLH) transcription factors were reduced, while secondary heart field genes were increased in expression early and were replaced by an increase in expression of cellular stress response genes later, suggesting a change in gene expression patterns or cell populations. Lineage tracing studies using *Mesp1*^{Cre} and *T-Cre* drivers showed that core mesoderm cells within PA1 were present at E9.5 but were greatly reduced by E10.5 in *Tbx1*$^{-/-}$ embryos. Using *Tbx1*^{Cre} knock-in mice, we found that cells are lost due to apoptosis, consistent with increase in expression of cellular stress response genes at E10.5. To determine whether *Tbx1* is required autonomously in the core mesoderm, we used *Mesp1*^{Cre} and *T-Cre* mesodermal drivers in combination with inactivate *Tbx1* and found reduction or loss of branchiomeric muscles from PA1. These mechanistic studies inform us that *Tbx1* is required upstream of key myogenic genes needed for core mesoderm cell survival and fate, between E9.5 and E10.5, resulting in formation of the branchiomeric muscles.

INTRODUCTION

Velo-cardio-facial syndrome (MIM # 192430)/DiGeorge syndrome (MIM# 188400), also known as 22q11.2 deletion syndrome (22q11DS), is caused by a 1.5–3 million base pair hemizygous 22q11.2 deletion and is characterized by cardiac, immune and craniofacial anomalies. Craniofacial malformations consist of submucous or overt cleft palate, platybasia and velo-pharyngeal insufficiency (VPI) (1–3). VPI symptoms include feeding or swallowing difficulties during infancy and hypernasal speech later. One cause of VPI is the existence of a submucous cleft palate and/or muscle hypotonia, both present in most 22q11DS patients (3–5). In addition to VPI, some 22q11DS children have asymmetric crying facies, which is characterized by drooping of one side of the mouth during crying. It is thought that this phenotype is caused in part by branchiomeric muscle hypoplasia (6).

The branchiomeric muscles are specific to the head and neck, but do not include extraocular muscles or the tongue. When compared with the somites in the body, branchiomeric muscles derive

*To whom correspondence should be addressed. Email: bernice.morrow@einstein.yu.edu
†These two authors contributed equally to the manuscript.

from unsegmented cranial paraxial mesoderm in the central core of the pharyngeal arches during embryogenesis (7,8). The core mesoderm cells within pharyngeal arch 1 (PA1) form the muscles of mastication required for chewing. Basic helix–loop–helix (bHLH) transcription factors are central to branchiomeric myogenesis. Four bHLH transcription factor genes, *Tcf21* (*Capsulin*), *Msc* (*MyoR*), *Myf5* and *MyoD*, play a critical role in craniofacial muscle formation. *Tcf21* and *Msc* work redundantly to regulate the first step of the specification of the branchiomeric muscles; in their combined absence, the muscles do not form from the core mesoderm *Tcf21* and *Msc* act upstream of *Myf5* and *MyoD* needed for differentiation (9,10).

In addition to the bHLH transcription factors, additional transcription factor genes play critical roles in forming the branchiomeric muscles and they include *Pitx2* and *Isl1* (11–16). *Pitx2* is required early for craniofacial muscle development (14,15). *Lhx2* encodes another homeodomain transcription factor required for branchiomeric muscle development (17). Thus far, *Tcf21*, *Msc*, *Pitx2*, *Isl1* and *Lhx2* are the known key transcription factor genes required for early craniofacial muscle development upstream of *Myf5* and *MyoD*; none lies in the 22q11.2 region deleted in affected individuals.

The *TBX1* gene is located within the 22q11.2 region that is hemizygously deleted in patients. It encodes a transcription factor that is part of the T-box gene family. Haploinsufficiency of *TBX1* is believed to be responsible for most of the physical defects in 22q11DS patients, including craniofacial anomalies (18–20). Mouse models have been useful in dissecting *Tbx1* function during embryogenesis. $Tbx1^{+/-}$ mice have mild defects at reduced penetrance, while $Tbx1^{-/-}$ mice die at birth with overt cleft palate and reduced or missing branchiomeric muscles, absent thymus and parathyroid glands and a single cardiac outflow tract instead of a separate aorta and pulmonary trunk (18–20). The distal pharyngeal arches do not form in $Tbx1^{-/-}$ mutant embryos, and thus, their derivatives do not form. The first pharyngeal arch is the only one present in mutant embryos and it appears grossly normal. The muscles of mastication form from the mandibular portion of pharyngeal arch one (PA1) and include the masseter, pterygoid and temporalis muscles, which are intermittently absent in $Tbx1^{-/-}$ embryos (21). Relevant to this, mouse genetic studies suggest that *Tbx1* acts downstream of *Tcf21*, *Pitx2* and *Isl1* and upstream of *Lhx2*, *Myf5* and *MyoD* (14,17,21,22). *Tbx1* is not required for initial core mesoderm formation or specification, because core mesodermal cells are present at E9.5, but it is required later to pattern the muscles (21). The mechanism responsible for craniofacial muscle loss in *Tbx1* mutant embryos is unknown.

Major goals here are to identify new genes and pathways downstream of *Tbx1* so as to determine why the muscles of mastication do not form in PA1 and finally, whether *Tbx1* is required cell autonomously, as was raised in the past for chick (23), but not conclusively proved in mouse models. We found that *Tbx1* is required for determining cell fate as well as survival, between E9.5 and E10.5, in the core mesoderm needed autonomously to form the muscles of mastication. This provides mechanistic evidence explaining why the craniofacial muscles do not form when *Tbx1* is inactivated.

RESULTS

Expression of PA1 core mesoderm genes reduced in $Tbx1^{-/-}$ embryos

In situ hybridization was performed on *Tcf21*, *Msc*, *Myf5* and *MyoD* in $Tbx1^{+/+}$ and $Tbx1^{-/-}$ mutant embryos at E9.5 (somites, 20–25) and E10.5 (somites, 30–35) as shown in Figure 1. Whole-mount *in situ* hybridization at E10.5 was followed by analysis of tissue sections to visualize the pattern of expression inside the embryos (Fig. 1). Expression appeared to be in the core mesoderm. All the four genes were expressed in PA1 at both stages in $Tbx1^{+/+}$ embryos, except *MyoD*, whose expression was not detected in PA1 at E9.5 (Fig. 1). The *Tcf21* and *Msc* genes were expressed in PA1 in $Tbx1^{-/-}$ embryos at E9.5, but not E10.5 (Fig. 1). In contrast, *Myf5* was absent in null mutant embryos at E9.5 and E10.5 (Fig. 1). Frontal whole-mount images are shown depicting gene expression patterns with respect to *Tbx1* showing expression of the four bHLH genes in a similar region of PA1 (Fig. 1).

To build molecular connections between *Tbx1* and the four bHLH genes as well as to identify new genes for branchiomeric myogenesis, gene expression profiling was performed from microdissected PA1 tissues from $Tbx1^{+/+}$ and $Tbx1^{-/-}$ mutant embryos at E9.5. We did not perform microarray analysis on $Tbx1^{+/-}$ embryos because they have no obvious craniofacial muscle defects (21,24). We first examined genes that were reduced in expression in the microarrays (Supplementary Material, Table S1). Ingenuity pathway analysis (IPA) and hand curation was done to create a gene network as shown in Figure 2A. The gene network included the genes that were reduced in expression in $Tbx1^{-/-}$ embryos (gray fill; Fig. 2A), the four bHLH genes discussed above (Fig. 1) and connecting genes identified by IPA irrespective of known function (Fig. 2A). We also evaluated gene expression levels in PA1 by quantitative reverse transcriptase–polymerase chain reaction (qRT–PCR; Fig. 2B). There are some differences between *in situ* hybridization, microarray and qRT–PCR results, but overall they showed a consistent differential expression pattern. For example, expression of *Tcf21* as detected by whole-mount *in situ* hybridization was not visibly changed in $Tbx1^{-/-}$ embryos at E9.5, but was lost in mutant embryos at E10.5 (Fig. 1). In contrast, *Tcf21* expression was significantly reduced in $Tbx1^{-/-}$ embryos by microarray (Supplementary Material, Table S1) and qRT–PCR (Fig. 2B) analyses at E9.5 and E10.5. *MyoD* expression was not detected by *in situ* hybridization analysis of $Tbx1^{+/+}$ embryos, nor was expression detected in the microarrays at E9.5 (somites 20–25). *MyoD* probes failed in the microarray at E10.5, possibly due to technical problems with the specific probe. Expression of *MyoD* was detected by qRT–PCR and it was reduced in $Tbx1^{-/-}$ embryos at E9.5 and E10.5 (Fig. 2B).

The IPA network contains genes that have been previously found to be genetically or molecularly connected to the differentially expressed genes in this study, but they may not show expression change in our system. This is because the IPA network builds connections based upon genes and their relationships from papers reported in the literature. For example, *Shh* and *Ash2l* were part of the IPA network but were not changed in expression by microarray or qRT–PCR. We included a list of top

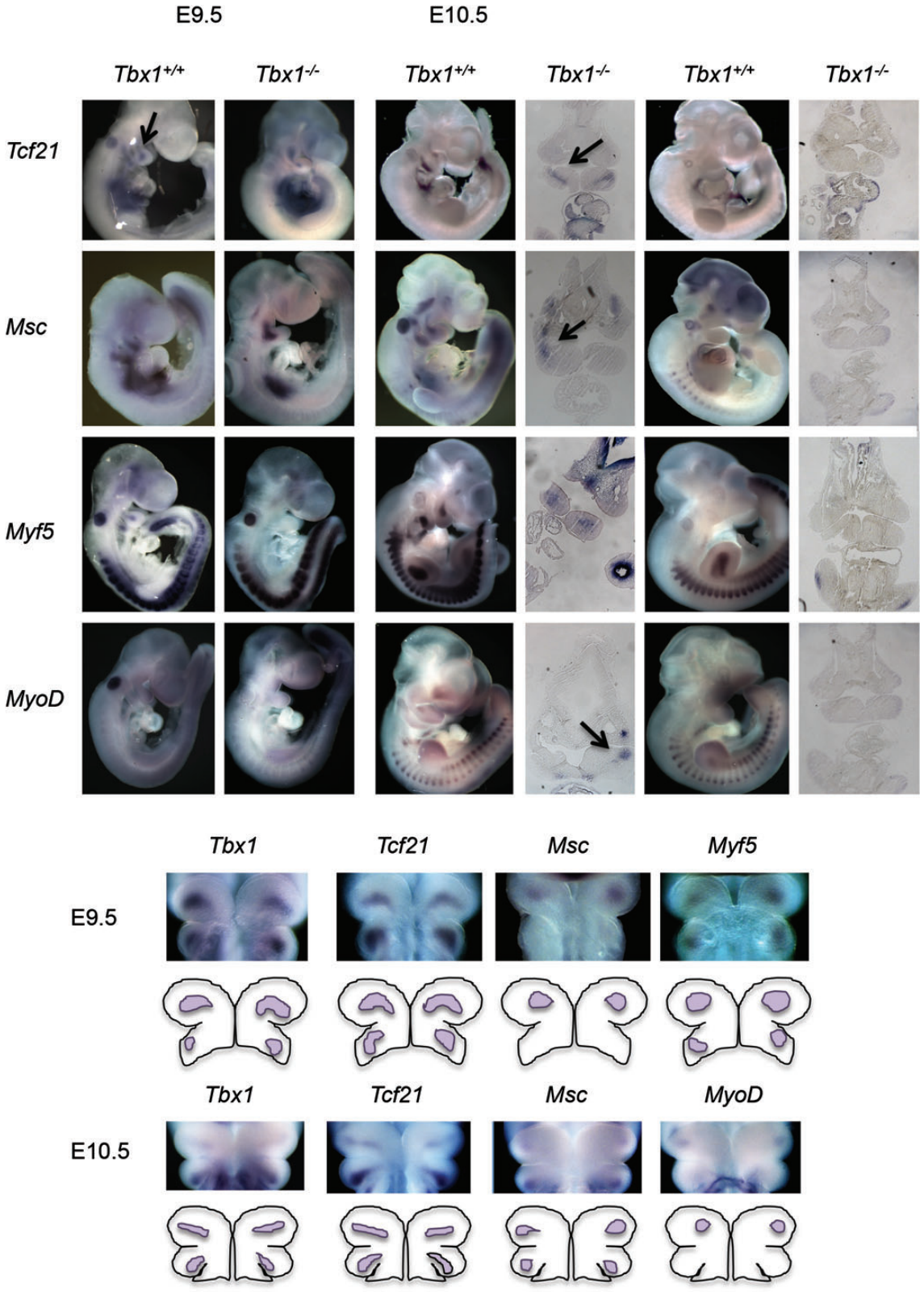

Figure 1. Basic HLH transcription factor genes, *Tcf21*, *Msc*, *Myf5* and *MyoD*, in $Tbx1^{+/+}$ versus $Tbx1^{-/-}$ embryos at E9.5 and E10.5. Lateral views of $Tbx1^{+/+}$ versus $Tbx1^{-/-}$ embryos at E9.5 (somite count, 20–25) and E10.5 (somite count, 30–40) are shown following whole-mount *in situ* hybridization with probes for *Tcf21*, *Msc*, *Myf5* and *MyoD.* Coronal histological sections of the PA1 region from E10.5 embryos are shown next to the whole-mount images. Arrow points to core mesoderm expression domain of *Tcf21* in PA1. The image below shows whole-mount coronal views of the first and second pharyngeal arch in $Tbx1^{+/+}$ embryos at E9.5 and E10.5 after whole-mount *in situ* hybridization, using antisense probes to the four bHLH genes. Cartoons are shown below to depict expression patterns of individual probes.

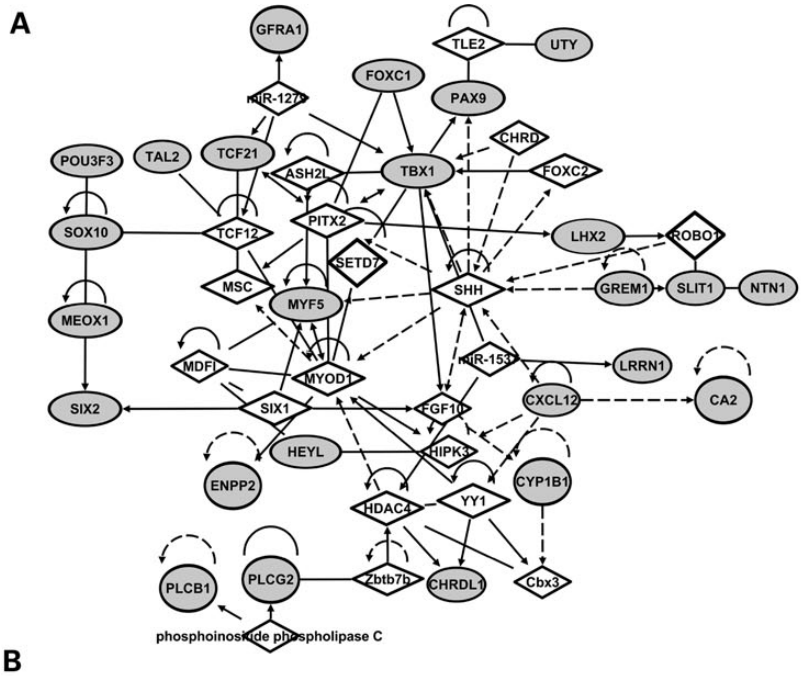

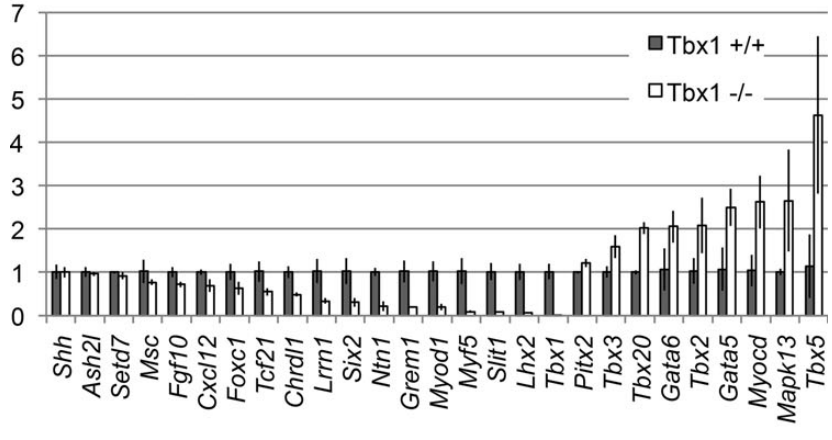

C

Feature	FDR	Genes in network	Genes in genome
Embryonic organ morphogenesis	5.10E-12	16	215
Sequence-specific DNA binding RNA polymerase II transcription factor activity	6.28E-10	14	203
Mesenchymal cell differentiation	9.03E-09	11	118
Autonomic nervous system development	1.28E-08	8	39
Mesenchyme development	2.40E-08	11	135
Mesenchymal cell development	4.93E-08	10	107
Cell fate commitment	5.76E-08	12	200
Neural crest cell development	5.76E-08	8	50
Neural crest cell differentiation	1.24E-07	8	56
Regionalization-embryo	2.54E-07	13	291
Sequence-specific distal enhancer binding RNA polymerase II transcription factor activity	3.85E-07	9	99

Figure 2. Gene network of PA1 genes reduced in expression at E9.5 in $Tbx1^{-/-}$ embryos. (**A**) The network of genes that were reduced in expression in $Tbx1^{-/-}$ embryos when compared with $Tbx1^{+/+}$ embryos (>1.5-fold change, $P < 0.05$) was created using IPA (http://www.ingenuity.com/products/ipa). The top network is depicted here. The genes reduced in expression are highlighted by gray fill, and additional genes connected to them based on IPA network analysis are indicated as diamonds. The lines indicate relationships between genes that could directly or indirectly interact. Genes reduced in expression but not linked to this network can be found in the Supplementary Material, Table S1. (**B**) Quantitative RT-PCR of PA1 tissue from $Tbx1^{+/+}$ and $Tbx1^{-/-}$ embryos at E9.5. The *X*-axis indicates genes analyzed and *Y*-axis represents fold change of expression in PA1 tissue from $Tbx1^{-/-}$ relative to $Tbx1^{+/+}$controls at E9.5. Error bars, s.e.m. ($n = 3$). (**C**) Genes reduced in expression in $Tbx1^{-/-}$ embryos at E9.5 were analyzed at the Genemania website (http://www.genemania.org/) to identify top enriched functions. We provide the FDR (false discovery rate) score estimated in Genemania by the Benjamini–Hochberg correction.

gene ontology networks identified from IPA analysis (Fig. 2C). The most significant category identified was embryonic organ morphogenesis with 16 of 215 genes connected to this particular network (Fig. 2C). Similarly, genes important for mesenchymal and neural crest cell development were reduced in expression (Fig. 2C).

We performed a similar gene profiling experiment at E10.5 to determine whether the same or different genes were reduced in expression (Supplementary Material, Table S2). We found that 20 genes were changed similarly between $Tbx1^{+/+}$ and $Tbx1^{-/-}$ embryos at stages E9.5 and E10.5. A subset of genes changed in the microarray as well as the four bHLH genes were tested by qRT–PCR (Supplementary Material, Fig. S1; Supplementary Material, Table S2). The qRT–PCR results (Supplementary Material, Fig. S1) were consistent with the microarray results, except for the expression of *Msc* and *MyoD*, for which were not significantly changed (or detected; *MyoD*) by microarray analysis, but there expression was reduced by qRT–PCR analysis. Based upon the gene lists from E9.5 and E10.5 (Supplementary Material, Tables S1 and S2) and qRT–PCR analysis (Fig. 2B; Supplementary Material, Fig. S1), we performed *in situ* hybridization to detect patterns of *Foxc1*, *Foxc2*, *Sim2*, *Lhx2*, *Lrrn1* and *Chrdl1* gene expression in $Tbx1^{+/+}$ and $Tbx1^{-/-}$ embryos.

We evaluated the spatial and temporal pattern of expression of these six genes in PA1 at E9.5 and E10.5. We separated the analysis to those known to be expressed in the core mesoderm from those expressed in the neural crest mesoderm. Two of the genes, *Lhx2* and *Lrrn1*, were expressed in the core mesoderm at E9.5 and three of the genes, *Lhx2*, *Chrdl1* and *Lrrn1*, were expressed at E10.5 in $Tbx1^{+/+}$ embryos (Fig. 3). The gene *Lhx2* encodes a LIM homeobox transcription factor that is required for craniofacial muscle formation. Recent studies showed that *Lhx2* acts downstream of *Tbx1*, *Pitx2* and *Tcf21* in the core mesoderm for branchiomeric muscle formation (17); however, we wanted to check expression in our *Tbx1* mutant allele. Expression of the *Pitx2* gene, although not changed in the PA1 microarray study, was slightly but significantly increased by qRT–PCR analysis (Fig. 2B). This data was included in the network shown in Figure 2A. *Lhx2* was expressed in the core mesoderm in $Tbx1^{+/+}$ embryos at E9.5 and E10.5 but absent from PA1 in $Tbx1^{-/-}$ embryos at both stages (Fig. 3).

The *Lrrn1* (neuronal leucine-rich repeat-1, *NLRR-1*) gene encodes a transmembrane glycoprotein localized on the cell surface. The gene is expressed in developing somites (25). The *Lrrn1* gene was weakly expressed in the core mesoderm of PA1 in $Tbx1^{+/+}$ embryos at E9.5 and strongly expressed at E10.5. Expression of *Lrrn1* was absent in $Tbx1^{-/-}$ embryos at E9.5 and E10.5 (Supplementary Material, Tables S1 and 2; Fig. 3). Of interest, a previous report demonstrated that *Lrrn1* expression was reduced in $MyoD^{-/-}$ myogenic cells in culture (26). This suggests a possible functional role of *Lrrn1* in branchiomeric myogenesis.

The *Chrdl1* (*Chordin like 1*) gene is a closely related Bone morphogenic protein (*Bmp*) antagonist gene family member to

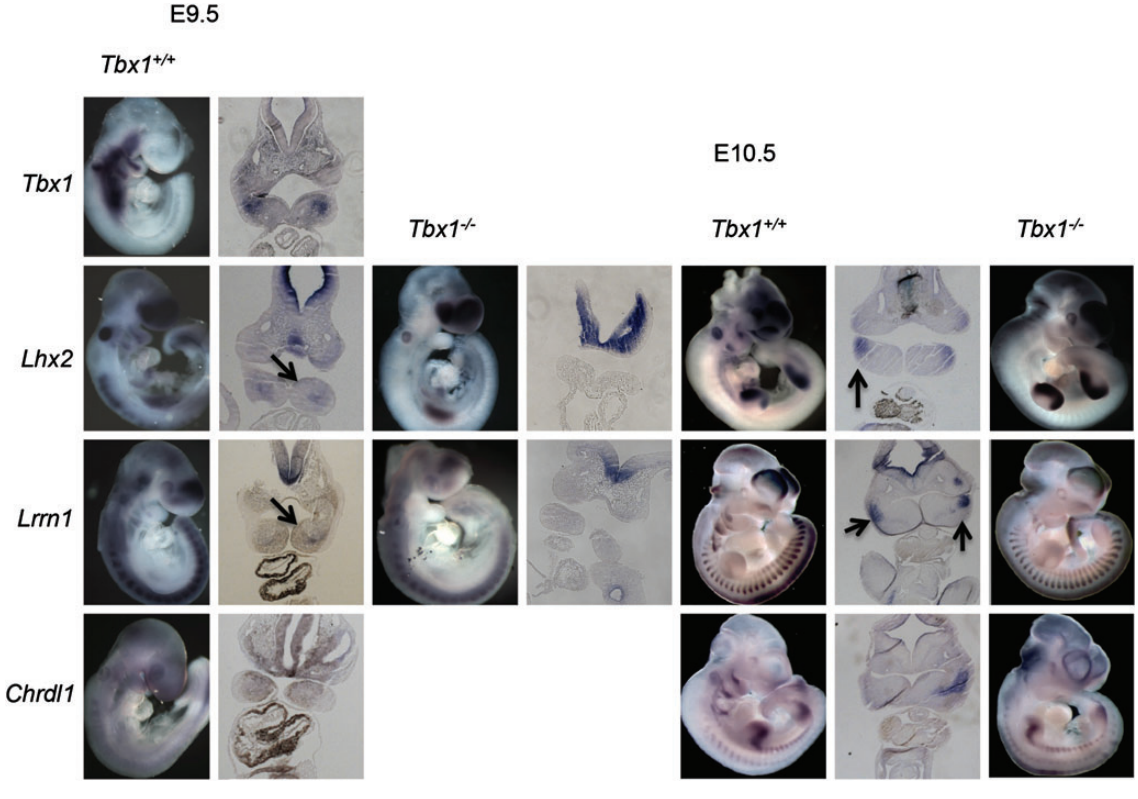

Figure 3. *Tbx1*, *Lhx2*, *Lrrn1* and *Chrdl1* expression in the core mesoderm in $Tbx1^{+/+}$ versus $Tbx1^{-/-}$ embryos at E9.5 and E10.5. Lateral views of whole-mount *in situ* hybridization of $Tbx1^{+/+}$ and $Tbx1^{-/-}$ embryos at E9.5 and E10.5 with antisense probes for *Tbx1* (Wt only), *Lhx2*, *Lrrn1* and *Chrdl1*. Coronal tissue sections from a subset of the whole-mount stained embryos are shown adjacent to the whole-mount images. *Chrdl1* is not expressed in the core mesoderm in $Tbx1^{+/+}$ embryos at E9.5; thus, no images are shown for $Tbx1^{-/-}$ embryos at this stage. *Lhx2*, *Lrrn1* and *Chrdl1* were not expressed in the core mesoderm in $Tbx1^{-/-}$ embryos so only whole-mount images are shown.

Chordin (27). *Chrdl1* is expressed in the neural plate, forebrain and pharyngeal apparatus core mesoderm among other tissues (27). *Chrdl1* was not specifically expressed in PA1 in $Tbx1^{+/+}$ embryos at E9.5 as determined by *in situ* hybridization analysis (Fig. 3). Although we did not find specific PA1 expression by *in situ* hybridization in $Tbx1^{+/+}$ embryos at E9.5, core PA1 expression was observed in a different report (26). This difference could be due to slight embryo stage differences, mouse strain or probe quality differences. On the other hand, specific PA1 expression by this method was observed at E10.5 (Fig. 3), similar to what was previously reported (26). PA1 expression was lost in $Tbx1^{-/-}$ embryos at E10.5, although forelimb bud expression remained (Fig. 3). *Chrdl1* expression as determined by microarray and qRT–PCR analysis was present in PA1 of $Tbx1^{+/+}$ embryos at E9.5 and E10.5 and it was reduced in $Tbx1^{-/-}$ embryos at both stages (Supplementary Material, Tables S1 and 2; Fig. 2B; Supplementary Material, Fig. S1).

The *Fgf10* gene, important downstream of *Tbx1* in multiple tissues, was previously shown to be expressed in the core mesoderm of the pharyngeal arches (28,29) and is part of the gene network shown in Figure 2A. *Fgf10* shows a very small reduction of expression in PA1 in $Tbx1^{-/-}$ embryos by microarray analysis (Supplementary Material, Table S1) and qRT–PCR at E9.5 (Fig. 2B). Consistent with this, we previously found that *Fgf10* is present in the core mesoderm in $Tbx1^{+/+}$ embryos but diffusely expressed in PA1 tissue of $Tbx1^{-/-}$ embryos at E9.5, rather than being absent (30).

Reduced expression of genes for craniofacial development in $Tbx1^{-/-}$ embryos

Neural crest cell (NCC) mesoderm lies in the first pharyngeal arch between the core mesoderm and surrounding epithelia. The *Foxc1* and *Foxc2* genes encode proteins that belong to the forkhead family of transcription factors. Both genes act redundantly for cardiac and vascular development in neural crest mesoderm as well as somitogenesis (31). As mentioned above, we found that expression of the *Foxc1* gene was reduced in $Tbx1^{-/-}$ when compared with $Tbx1^{+/+}$ embryos at E9.5 and E10.5 by both microarray and qRT–PCR analyses (Supplementary Material, Figs S1 and 2B). We performed *in situ* hybridization to determine whether the pattern of expression changed in $Tbx1^{-/-}$ embryos at E9.5 and at E10.5. The *Foxc1* gene was broadly expressed in $Tbx1^{+/+}$ embryos at E9.5 and more specifically expressed in the caudal PA1 at E10.5 (Fig. 4A and B). Expression was similar between $Tbx1^{+/+}$ when compared with $Tbx1^{-/-}$ embryos at E9.5, but localized to a smaller region in $Tbx1^{-/-}$ embryos at E10.5 (Fig. 4A).

In contrast to *Foxc1*, we did not detect a change in expression of *Foxc2* at E9.5 in the microarray experiment (Supplementary Material, Table S1) and did not perform qRT–PCR at this stage. We observed a similar diffuse pattern of expression in PA1 for *Foxc2*, as for *Foxc1* in $Tbx1^{+/+}$ and $Tbx1^{-/-}$ embryos by *in situ* hybridization at E9.5 (Fig. 4A). Consistent with microarray and qRT–PCR findings (Supplementary Material, Table S2 and Fig. S1), there was loss of expression in PA1 at E10.5 in $Tbx1^{-/-}$ embryos by *in situ* hybridization analysis (Fig. 4A; Supplementary Material, Fig. S1).

The *Sim2* gene encodes a bHLH transcription factor gene (*single-minded*, *Drosophila*) expressed in the pharyngeal

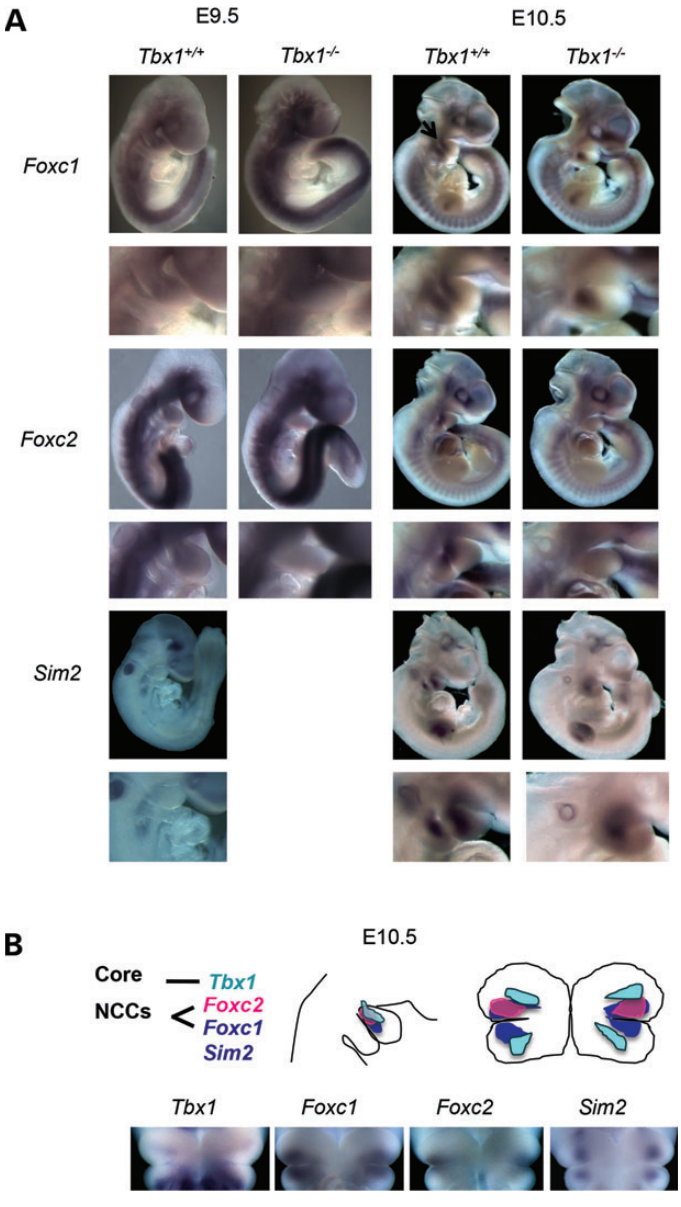

Figure 4. *Foxc1*, *Foxc2* and *Sim2* expression in PA1 in $Tbx1^{+/+}$ versus $Tbx1^{-/-}$ embryos at E9.5 and E10.5. (**A**) Lateral views of whole-mount *in situ* hybridization of probes for *Foxc1*, *Foxc2* and *Sim2 in* $Tbx1^{+/+}$ and $Tbx1^{-/-}$ embryos at E9.5 and E10.5. Enlarged lateral views of the PA1 region in the whole-mount specimens is shown below each whole embryo view. (**B**) Cartoon of lateral and coronal views (shown below) of *Tbx1*, *Foxc1*, *Foxc2* and *Sim2*. Expression domain of *Tbx1* is in the core mesoderm.

arches and is required to form the secondary palate, tongue and pterygoid process (32). The muscles of mastication are still present in $Sim2^{-/-}$ mutant mice, and thus, it is not required for branchiomeric myogenesis (32). We did not observe expression of *Sim2* by *in situ* hybridization or microarray analysis in $Tbx1^{+/+}$ embryos at E9.5 (Fig. 4A). *Sim2* is expressed in the pharyngeal arches at E10.5 in $Tbx1^{+/+}$ embryos. It appears to be adjacent to the *Tbx1* expression domain, although we cannot rule out that *Sim2* expression may partially overlap with that of *Tbx1* (Fig. 4B). The area of expression is reduced in $Tbx1^{-/-}$ embryos but not absent at this stage (Fig. 4). At E10.5, expression of *Sim2*, as determined by microarray (Supplementary Material,

Table S2) and qRT–PCR (Supplementary Material, Fig. S1) analysis, was reduced in *Tbx1*$^{-/-}$ embryos. The specific patterns of expression in PA1 tissue of *Foxc1*, *Foxc2*, *Sim2* and *Tbx1* are shown in lateral and frontal views in the cartoon in Figure 4B. Changes in expression of all three genes implicate possible roles downstream of *Tbx1* in either craniofacial muscle and/or bone development.

Increased expression of PA1 genes in *Tbx1*$^{-/-}$ embryos

We examined genes increased in expression in *Tbx1*$^{+/+}$ versus *Tbx1*$^{-/-}$ mutant embryos at E9.5 by gene expression microarray analysis (Fig. 5). As for genes reduced in expression described above, we performed gene network analysis (Fig. 5A). Many of the genes increased in expression at E9.5 (gray fill; Fig. 5A) are known genes for cardiac development and differentiation (Fig. 5B). A subset of the genes that were increased in expression in the microarray in *Tbx1*$^{-/-}$ mutant embryos at E9.5 were tested and confirmed by qRT–PCR of dissected PA1 tissue (Fig. 2B). Based upon the results, it is possible that loss of *Tbx1* results in a change in fate of the core mesoderm from the craniofacial pattern to the cardiac differentiation program. To test this, we performed *in situ* hybridization analysis. Ectopic expression of *Gata4*, *Gata5*, *Gata6* and *Tbx20* transcription factor genes extended rostrally to the caudal tip of PA1, but were not detected in the core mesoderm (Fig. 5C). This suggests that increase in expression may not be due to cell fate change in the core mesoderm from the craniofacial to the cardiac specific developmental pathways. Furthermore, additional cardiac specific genes were also ectopically expressed rostrally in *Tbx1*$^{-/-}$ embryos, such as *Myl7*, *Actc1* and *Tbx5* (33). They were expressed in the caudal part of PA1 but were not detected in the core mesoderm (33).

At E10.5, we found a different set of genes increased in expression by gene profiling of PA1 tissue in *Tbx1*$^{-/-}$ embryos versus *Tbx1*$^{+/+}$ embryos. We detected enrichment of stress response and glucose metabolism genes (Fig. 6). Four genes were increased in expression in the microarrays at E9.5 and E10.5 in PA1 tissue in *Tbx1*$^{-/-}$ embryos: *Mapk13*, *Rarres2*, *Lipg* and *Vldlr* (Supplementary Material, Table S2). We validated enhanced expression of *Mapk13* at E9.5 and E10.5 in *Tbx1*$^{-/-}$ mutant embryos by qRT–PCR, albeit with some differences in the extent of upregulation in expression between microarray and the qRT–PCR assays (Fig. 2B; Supplementary Material, Fig. S1). *Mapk13* encodes mitogen-activated protein kinase 13 (p38 delta) and it is important for promoting cell survival in response to cell stress (34). *Rarres2* encodes a retinoic acid receptor responder (tazarotene induced) 2, also referred to as Chemerin, an adipokine, and is a retinoic acid responsive gene (29). *Lipg* encodes a lipase and *Vldlr* encodes very low density lipoprotein receptor and it is upregulated in response to hypoxia (35). Several genes increased in expression belong to the Vegf, hypoxia response pathway and Akt, cellular survival pathways as indicated (Fig. 6). This may implicate the presence of cellular stress or apoptosis.

Core mesodermal tissue is lost in *Tbx1*$^{-/-}$ embryos between E9.5 and E10.5

To determine the embryonic stage when tissue forming these muscles is reduced or lost in *Tbx1*$^{-/-}$ mutant embryos, we crossed *T-Cre*; *Mesp1*$^{Cre/+}$; *Tbx1*$^{+/-}$ mice with *RCE*$^{EGFP/EGFP}$; *Tbx1*$^{+/-}$ mice and dissected embryos to perform lineage tracing. We combined the two mesodermal Cre drivers together to ensure more complete fate mapping of the lineage (*Meso-Cre*). Fortunately, neither *T-Cre* nor *Mesp1*$^{Cre/+}$ results in ectopic loxP site recombination *in vivo* (28,36). At E9.5, the mesodermal lineage was seen in the pharyngeal apparatus and heart, as expected (Fig. 7I–P). Core mesodermal tissue was apparent in PA1 in *Tbx1*$^{+/+}$ and *Tbx1*$^{-/-}$ embryos (Fig. 7K, L, O and P). Existence of core mesodermal cells (21) is supported by the presence of *Tcf21* and *Msc* mRNA expression at E9.5 in *Tbx1*$^{-/-}$ embryos (Fig. 1).

The situation was different at E10.5, where the mesodermal lineage covered a larger area of the embryo, including the somites (Fig. 7A–D); however, the cell lineages were largely reduced or absent in the same region from *Tbx1*$^{-/-}$ embryos (Fig. 7E–H). This is consistent with loss of mRNA expression of all core mesodermal genes at E10.5 (Supplementary Material, Table S2). The results suggest that the core mesoderm cells are greatly reduced or lost between E9.5 and E10.5. We observed a small patch of unstained cells surrounded by robustly labeled NCCs in *Tbx1*$^{-/-}$ embryos using a *Wnt1-Cre* driver and a *ROSA26-LacZ* reporter to trace the NCCs in *Tbx1*$^{-/-}$ embryos at E10.5, indicating that at least some mesodermal cells are present, perhaps of a different lineage (28).

Increased apoptosis in the core mesoderm of *Tbx1*$^{-/-}$ embryos at E9.5–E10

To determine whether there is a change in cell proliferation or apoptosis accounting for loss of core mesodermal gene expression, we used *Tbx1*$^{Cre/+}$ mice (37) to perform lineage tracing. *Tbx1*$^{Cre/+}$ is a knock-in and there is a replacement of part of the *Tbx1* coding region with Cre recombinase on one allele, thereby inactivating *Tbx1* (37). Previous studies showed that proliferation of mesenchymal cells in the pharyngeal apparatus was reduced at E8.5 in *Mesp1*^{Cre}-mediated *Tbx1* conditional null mutant embryos (38), suggesting cell autonomous differences in proliferation early in development. We evaluated cell proliferation from E9.5 (S20–25) to E10.0 (S26–29) in *Tbx1*$^{Cre/+}$; *RCE*$^{EGFP/+}$ (heterozygous control) and *Tbx1*$^{Cre/-}$; *RCE*$^{EGFP/+}$ (mutant) embryos by dual immunofluorescence with antibodies against GFP and anti-phospho Histone H3 (Ser10). *Tbx1*$^{+/-}$ mice have no defects in craniofacial muscles, making it possible to use the knock-in line for comparative lineage tracing. We calculated the average number of *Tbx1* lineage cells (GFP fluorescence) and proliferating cells (Rhodamine fluorescence) per tissue section for heterozygous controls (WT; Fig. 8B) and mutant embryos (KO; Fig. 8B). At E9.5, heterozygous control embryos had similar numbers of *Tbx1* lineage and proliferating cells (19.3/section, 15.0/section; $n = 3$) with homozygous null mutant embryos (17.4/section, 14.5/section; $n = 4$). Closer to E10, heterozygous controls tended to have more *Tbx1* lineage cells than in homozygous mutant embryos (39.9/section, $n = 3$ versus.16.8/section, $n = 6$; $P = 0.12$), while proliferating cells were similar between the two genotypes (31.0/section; $n = 3$ versus. 33.1/section; $n = 6$). We noted qualitatively that proliferation occurred in few cells and evenly across the entire PA1 tissue in control and mutant embryos at E9.5 (S20–21; data not shown) and E9.5–

A

B

Feature	FDR	Genes in network	Genes in genome
cardiac muscle tissue development	2.53E-19	18	120
heart morphogenesis	3.96E-17	18	163
contractile fiber part	1.62E-16	16	118
contractile fiber	2.34E-15	16	141
cardiac chamber development	1.24E-14	14	98
sarcomere	3.26E-14	14	106
cardiac ventricle development	4.32E-14	13	83
cardiac chamber morphogenesis	1.02E-13	13	90
striated muscle tissue development	1.02E-13	18	272
muscle tissue development	1.94E-13	18	285
myofibril	3.05E-13	14	129
cardiac ventricle morphogenesis	9.34E-13	11	58
cardiac muscle tissue morphogenesis	1.11E-11	10	50
muscle tissue morphogenesis	3.49E-11	10	56

C

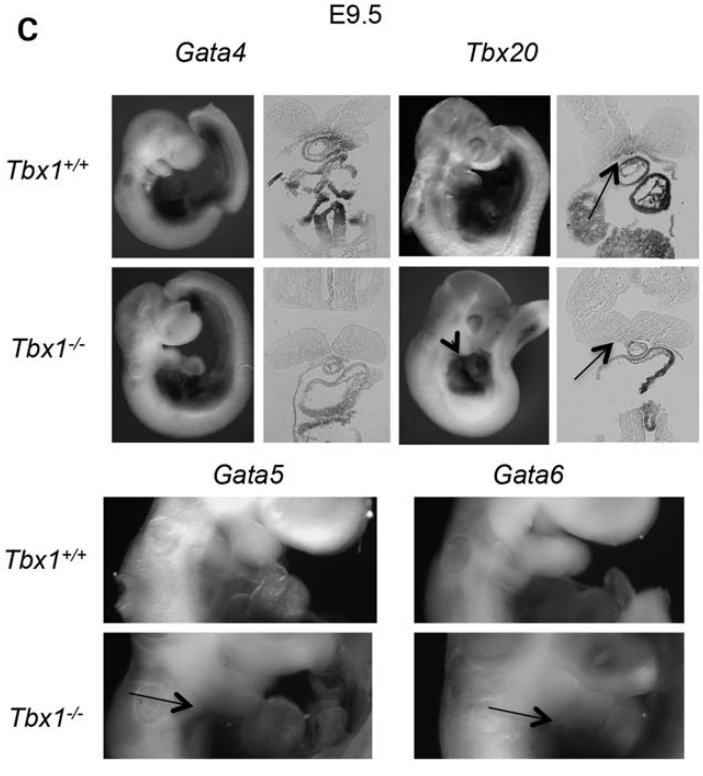

Figure 5. Ectopic expression of cardiac genes in PA1 in $Tbx1^{+/+}$ versus $Tbx1^{-/-}$ embryos at E9.5. (**A**) The network downstream of *Tbx1* was created using genes that had a >1.5-fold increase, $P < 0.05$ by microarray analysis (gray fill). Genes not changed in expression significantly in the microarray or qRT–PCR assay, but connected to those based upon the software generated connections, are indicated as uncolored circles. The lines indicate relationships between genes that could be direct or indirect in nature. Genes increased in expression but not linked to the network were removed but can be found in the Supplementary Material, Table S1. (**B**) Genes increased in expression in $Tbx1^{-/-}$ embryos at E9.5 were analyzed at the Genemania website to identify top enriched functions. We provide the FDR score estimated in Genemania by the Benjamini–Hochberg correction. (**C**) Whole-mount *in situ* hybridization was performed on in $Tbx1^{+/+}$ versus $Tbx1^{-/-}$ embryos at E9.5 with probes to the genes indicated. Tissue sections are shown adjacent to whole embryo images. The arrows in *Tbx20* images point to regions of ectopic expression. Regions of ectopic expression of *Gata5* and *Gata6* in $Tbx1^{+/+}$ versus $Tbx1^{-/-}$ embryos are shown as arrows in the cropped images.

A

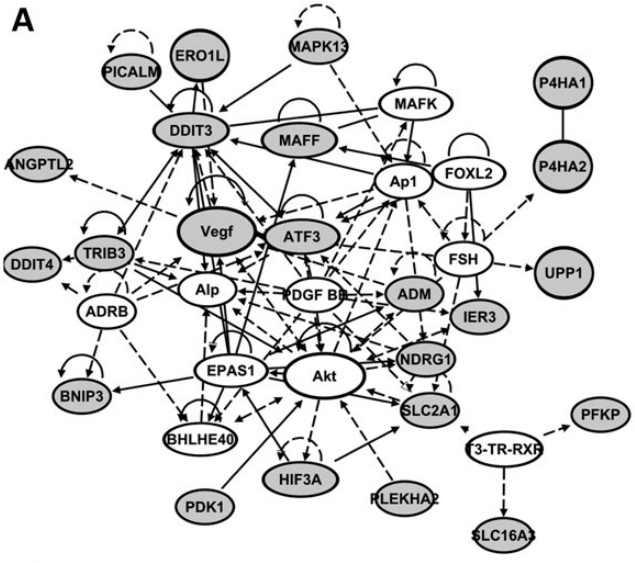

B

Feature	FDR	Genes in network	Genes in genome
glucose metabolic process	2.03E-06	9	138
glycolysis	2.43E-06	6	32
hexose metabolic process	2.55E-06	9	160
glucose catabolic process	7.99E-06	6	43
monosaccharide metabolic process	8.40E-06	9	198
hexose catabolic process	8.40E-06	6	46
monosaccharide catabolic process	1.04E-05	6	49
alcohol catabolic process	4.28E-05	6	63
cellular carbohydrate catabolic process	7.89E-05	6	71
carbohydrate catabolic process	1.58E-04	6	81
generation of precursor metabolites and energy	3.47E-04	7	156
response to hypoxia	9.59E-04	6	113
response to oxygen levels	1.09E-03	6	117
response to unfolded protein	4.33E-03	4	37
response to endoplasmic reticulum stress	5.01E-03	4	39
response to topologically incorrect protein	6.35E-03	4	42
small molecule catabolic process	9.24E-03	6	177
regulation of glycolysis	2.07E-02	3	19
cellular response to hypoxia	2.68E-02	3	21

Figure 6. Ectopic expression of hypoxia and stress response pathway genes in PA1 in $Tbx1^{+/+}$ versus $Tbx1^{-/-}$ embryos at E10.5. (**A**) The network of genes that were reduced in expression in $Tbx1^{-/-}$ embryos when compared with $Tbx1^{+/+}$ embryos (>1.5-fold change, $P < 0.05$) was created using IPA. The top network is depicted here. The genes increased in expression are highlighted in orange. The lines indicate relationships between genes that could directly or indirectly interact. Genes increased in expression but not linked to this network can be found in the Supplementary Material, Table S2. (**B**) Genes increased in expression in $Tbx1^{-/-}$ embryos at E10.5 were uploaded to the Genemania website to identify top enriched functions.

E10 (S24–26; Fig. 8). We therefore concluded that loss of *Tbx1* did not significantly affect PA1 cell proliferation at E9.5 or E10.

We next examined apoptosis using TUNEL assays on histological sections at E9.5 (S20–21; heterozygous controls, $n = 3$; mutant embryos, $n = 3$) and E9.5–10.0 (S23–26; heterozygous controls, $n = 5$; homozygous mutant embryos, $n = 6$), using the same approach as for proliferation analysis. We noted intense TUNEL staining in histological sections from homozygous mutant embryos at E9.5–E10 near the GFP cell lineage (Fig. 8). We observed a large, intense region of TUNEL staining in the center of the PA1 in the vicinity of the *Tbx1* lineage in $Tbx1^{Cre/-}$ mutant embryos that was not observed in heterozygous controls as shown in the representative image in Figure 8 and Supplementary Material, Figure S2. This suggests that there is loss of PA1 cells by apoptosis. When taken together with the *in situ* hybridization experiments, microarray, qRT–PCR analysis, lineage tracing and our previous report showing no difference in proliferation or apoptosis at E10.5 (28), current results suggest that core mesoderm cells are lost prior to E10.5 due to apoptosis.

Tbx1 is required in the core mesoderm to form muscles of mastication

It has been established that development of the branchiomeric muscles is disrupted in $Tbx1^{-/-}$ mutant embryos (21,24). Surprisingly, the muscles were present as normal, after inactivation of *Tbx1* using $Mesp1^{Cre}$ or *T-Cre* mesodermal drivers (23,28,38). Thus, inactivation of *Tbx1* was not complete using either allele alone (23,28,39). This is in contrast to the chick model where *Tbx1* is required in the mesoderm to promote craniofacial muscle formation (23). It is important to understand these differences, because it would help decipher molecular mechanisms. In mouse models, significant *Tbx1* expression remained in conditional mutant embryos using $Mesp1^{Cre}$ mice to drive mesodermal inactivation (38). It may be because of sub-optimal recombination of loxP sites or that different mesodermal lineages comprise the core mesoderm. To get around this problem, we crossed *T-Cre*; $Mesp1^{Cre/+}$; $Tbx1^{+/-}$ mice with $Tbx1^{flox/flox}$ mice to obtain $MesoTbx1^{flox/+}$ or $MesoTbx1^{flox/-}$ mice, which were heterozygous for both mesodermal drivers of *Cre*. The masseter, pterygoid and temporalis muscles were absent on both sides in one embryo (Supplementary Material, Fig. S3), absent on one side and hypoplastic on the other in another embryo (Fig. 9 and Supplementary Material, Fig. S3), and hypoplastic in both in a third and fourth embryos (Supplementary Material, Fig. S3). Variable penetrance of craniofacial muscles is similar to the situation in $Tbx1^{-/-}$ embryos (21). Resulting mutant embryos showed a major reduction of *Tbx1* expression in the mesoderm, although its expression was still not completely lost (Fig. 9B). The second and distal pharyngeal arches were missing in most mutant embryos ($MesoTbx1^{flox/-}$; Fig. 9C). *Myf5* expression, normally in the core mesoderm, was lost in the $MesoTbx1^{flox/-}$ embryos at E10.5 (Fig. 9C), indicating that mesoderm loss of *Tbx1* behaves similar to that of the global null mutant.

DISCUSSION

In this report, we attempted to understand the mechanistic basis for the loss of branchiomeric muscles in $Tbx1^{-/-}$ embryos. This is because once the mechanism is understood, we may be able to identify the molecular pathogenesis of muscle hypotonia in

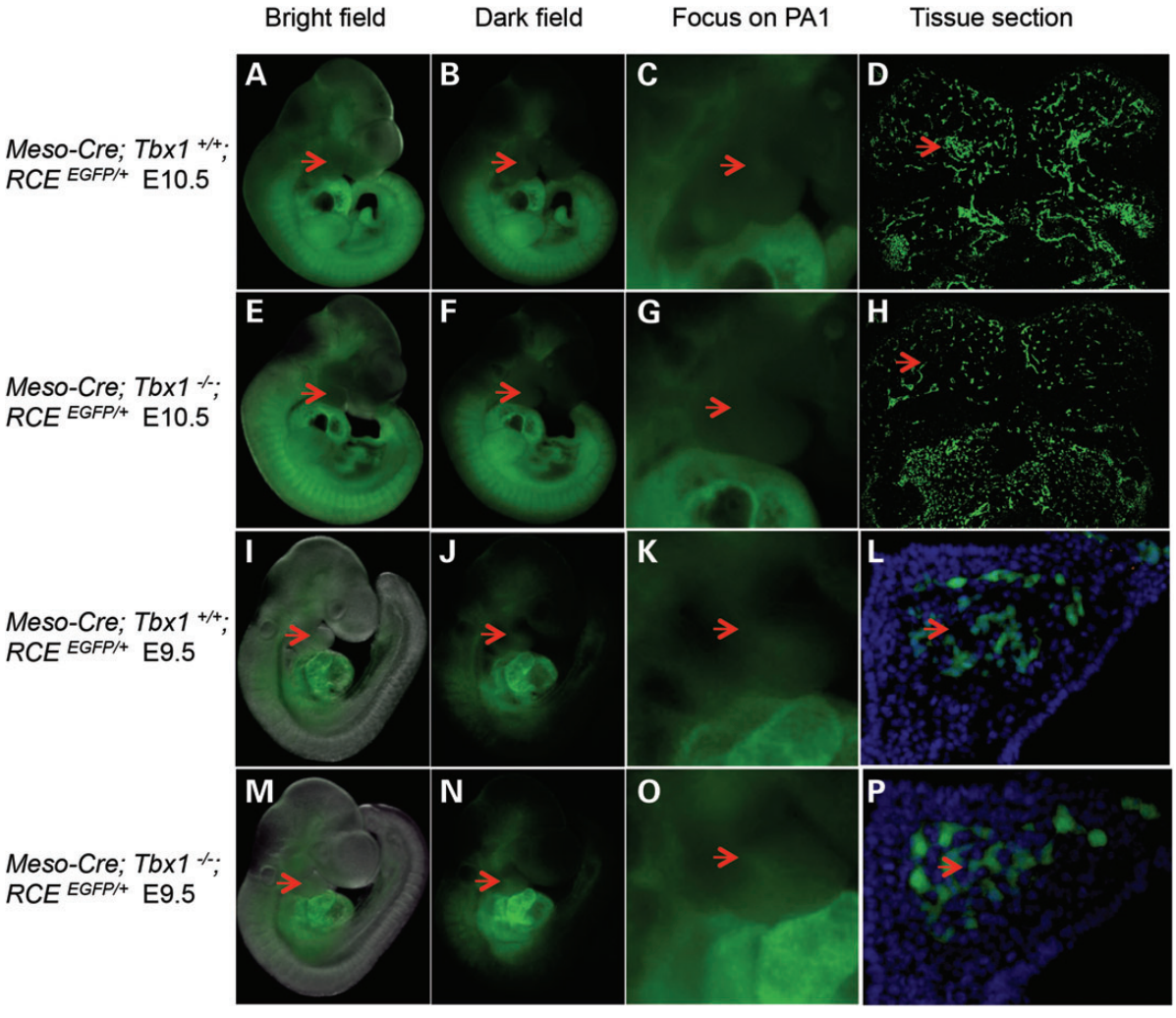

Figure 7. Mesodermal fate mapping in $Tbx1^{+/+}$ versus $Tbx1^{-/-}$ embryos at E9.5 and E10.5. Mesodermal fate mapping was performed using $Mesp1^{Cre}$ with *T-Cre* alleles and $RCE^{EGFP/+}$ mice in $Tbx1^{+/+}$ versus $Tbx1^{-/-}$ littermates at E9.5 (**I**–**P**) and E10.5 (**A**–**H**). Lateral views of $Tbx1^{+/+}$ (A–D and I–L) and $Tbx1^{-/-}$ (E–H and M–P) mutants are shown as bright (A, E, I and M) and darkfield (B, F, J and N) views. The red arrow points to the region of the presence or absence of core mesodermal tissue in $Tbx1^{+/+}$ versus $Tbx1^{-/-}$ at E9.5 and E10.5. An enlarged image of the PA1 region is shown to the right of the images (C, G, K and O). On the far right are coronal cryosections of the same embryos depicting the core mesodermal cells (D, H, L and P). Dapi stain was used to visualize PA1 at E9.5 (L and P).

22q11DS patients. In order to generate hypotheses for possible mechanisms, we performed gene profiling at two developmental stages, at E9.5 and at E10.5, which turned out to be critical stages for *Tbx1* function, because at these stages core mesodermal gene expression declines coincident with loss of cells due to apoptosis.

Tbx1 may be required to maintain *Tcf21* and *Msc* gene expression

We found that at stages E9.5 and/or E10.5, *Tcf21*, *Msc*, *Myf5* and *MyoD* were decreased in expression. This is somewhat surprising for *Tcf21*, especially at E9.5, since it is known that when *Tcf21* is inactivated *Tbx1* expression is reduced, suggesting that it acts downstream of *Tcf21* (17). This work suggests that *Tbx1* might be required to maintain *Tcf21* expression at E9.5 to E10.5. Expression of both *Tcf21* and *Msc* were absent from PA1 at E10.5. Our observation that *Tcf21* expression was lost in $Tbx1^{-/-}$ embryos at E10.5 is in contrast to a previous report indicating that *Tcf21* was still expressed in their $Tbx1^{-/-}$ mutant embryos at this stage (40). This discrepancy could be due to differences in somite counts for which ranges define stage, difference in alleles or to differences in genetic backgrounds. Overall, the new findings in this experiment are that *Tcf21* and *Msc* are reduced in expression at E10.5 in our $Tbx1^{-/-}$ embryos.

In previous studies, when mouse *Tcf21* and *Msc* were both inactivated, muscles of mastication did not form due to apoptosis of core mesoderm cells by E10.5 (41). The timing of both gene expression changes and enhanced apoptosis suggests that loss of tissue in $Tbx1^{-/-}$ null mutant embryos might be explained, in part, by failure to maintain *Tcf21* and *Msc* expression. This is because *Tcf21* and *Msc* act upstream of *Myf5* and *MyoD* and are required for survival of the core mesoderm (10). Reduction in *Myf5* and *MyoD* expression in $Tbx1^{-/-}$ mutant embryos could be a direct or indirect result of loss of *Tcf21* and *Msc*

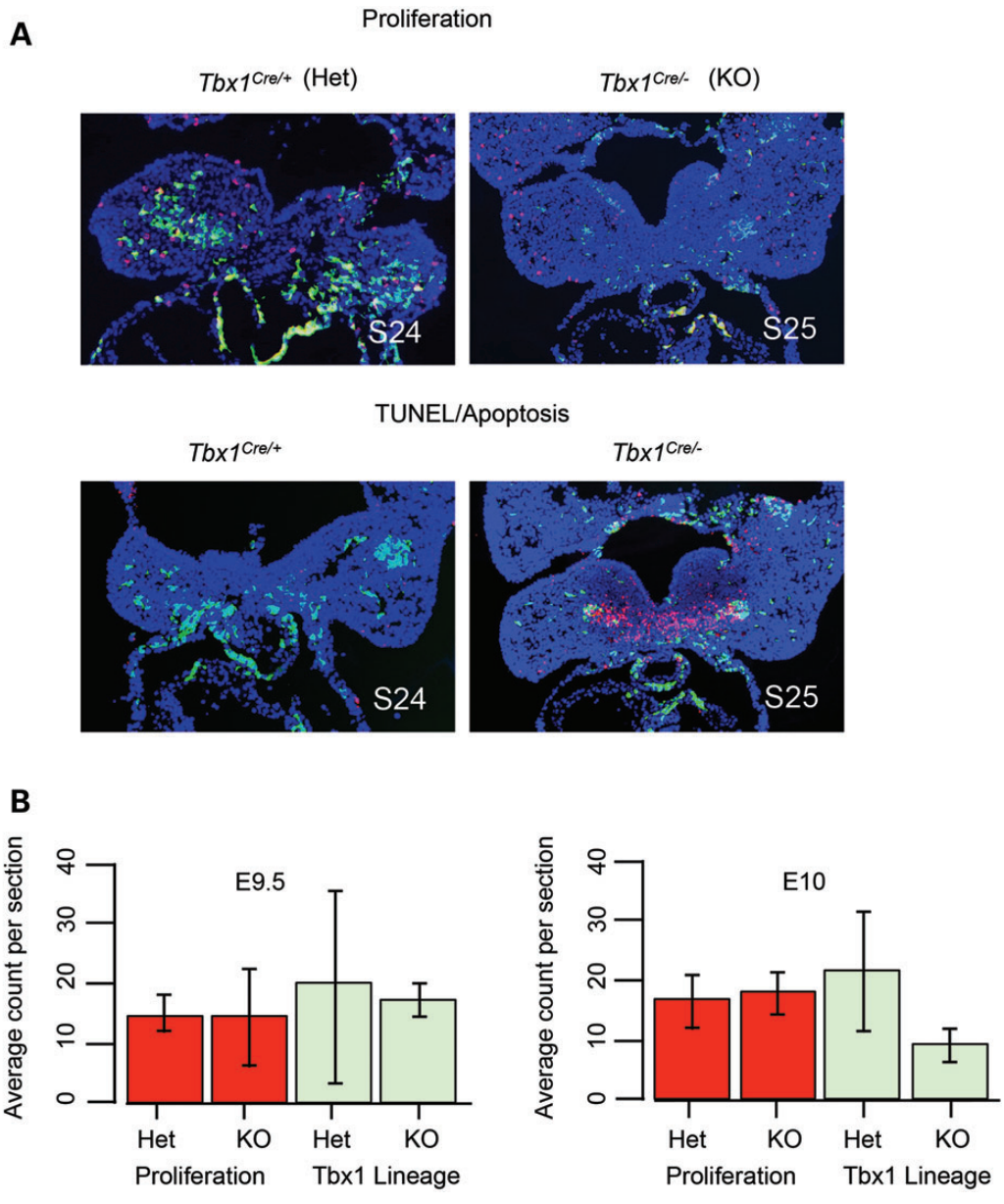

Figure 8. Proliferation and apoptosis of PA1 in *Tbx1*$^{+/+}$ versus *Tbx1*$^{-/-}$ embryos. (**A**) Immunofluorescence images of tissue sections to visualize the Tbx1 lineage (GFP, green) and either cell proliferation (anti-phospho Histone H3 (Ser10); red fluorescence; top) or apoptosis (TUNEL); red fluorescence; bottom) in *Tbx1* heterozygous (Het) and homozygous mutant (KO) embryos are shown. Dapi fluorescent stain to visualize nuclei and identify the tissue is shown in blue. The somite counts of the *Tbx1*$^{+/+}$ and *Tbx1*$^{-/-}$ embryos are indicated (S24; S25). (**B**) Cell proliferation analysis. Statistical analysis was performed to determine whether cell proliferation was the same or different between *Tbx1* heterozygous and homozygous null mutant embryos. The bar graph depicts average count per section with error bars from Student's *t*-test indicated.

expression. This would implicate direct or indirect transcriptional regulation of *Tcf21* and *Msc*. Relevant to this, it has remained an enigma in the field as to whether *Tbx1* has cell autonomous functions in the core mesoderm. In the chick model, downregulation of *Tbx1* in the core mesoderm tissue *in vitro* resulted in loss of branchiomeric muscles, but in the mouse model, use of single mesodermal drivers of Cre recombinase was unable to completely disrupt *Tbx1* resulting in continued presence of the muscles of mastication (23). By simultaneously using two different mesodermal Cre drivers, we were able to demonstrate that *Tbx1* has cell autonomous functions in promoting myogenesis in this tissue. This suggests that a main function of *Tbx1* is to maintain direct or indirect regulation of *Tcf21* and *Msc* expression, as well as other genes, in the core mesoderm of PA1.

One question is whether this is a direct effect or whether *Tbx1* in the mesodermal core indirectly signals to neural crest mesenchymal cells, which then inhibit myogenesis (21). Although we cannot directly answer this question, we do know that complete inactivation of *Tbx1* or partial inactivation of *Tbx1* using *T-Cre* mice (mesodermal inactivation) alters patterns of expression pattern of many neural crest expressed genes and results in ectopic expression of *Hoxa2* (28). However, the muscles of mastication still formed in *T-Cre* mediated *Tbx1* conditional mutants (28). When taken together, this suggests that changes in neural

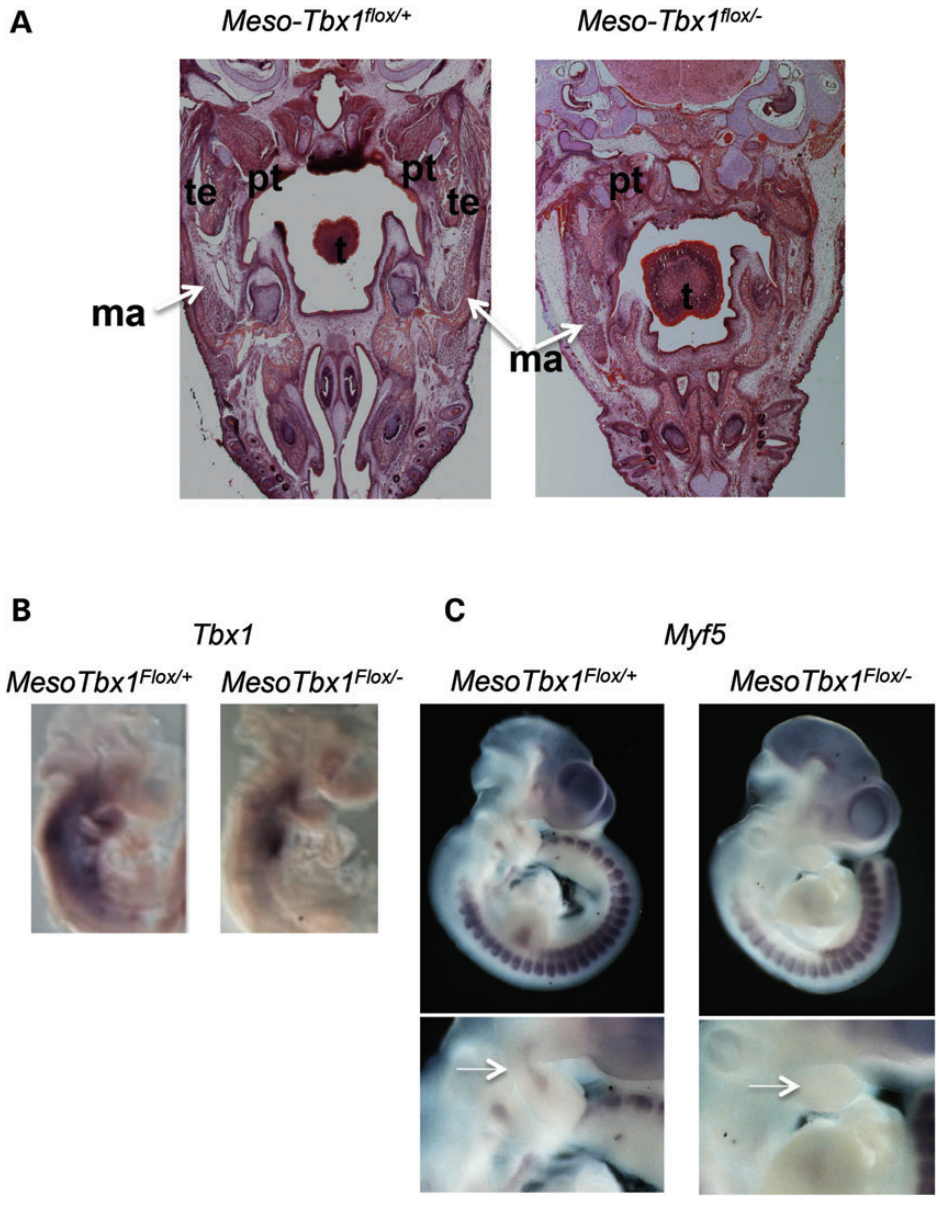

Figure 9. Mesodermal *Tbx1* is required to form the muscles of mastication. (**A**) Transverse histological sections of $Mesp1^{Cre/+}$; *T-Cre*; $Tbx1^{flox/+}$ and $Mesp1^{Cre/+}$; *T-Cre*; $Tbx1^{flox/-}$ (*MesoTbx1*$^{flox/+}$ or *MesoTbx1*$^{flox/-}$) embryos at E17.5 stained with hematoxylin and eosin. Adipocytes have largely replaced muscles of mastication (right). The masseter muscle is present unilaterally, but hypoplastic, and a pterygoid muscle is present unilaterally (additional images are in the Supplementary Material, Fig. S3), but again, is severely hypoplastic. ma = masseter. (**B**) Lateral views of whole-mount *in situ* hybridization of antisense probe for *Tbx1* in *MesoTbx1*$^{flox/+}$ and *MesoTbx1*$^{flox/-}$ littermates at E9.5. Mesodermal expression of *Tbx1* in heterozygous embryos is greatly reduced, but still present in conditional mutants. (**C**) Lateral views of whole-mount *in situ* hybridization of antisense probe for *Myf5* in *MesoTbx1*$^{flox/+}$ and *MesoTbx1*$^{flox/-}$ littermates at E10.5. Enlarged pharyngeal region from *in situ* hybridization images are shown below whole embryo views. Arrow points to the *Myf5* core mesoderm expression domain. Expression was diminished in conditional null mutant embryos.

crest mesenchymal gene patterns alone cannot account for loss of core mesoderm tissue, and likely *Tbx1* has cell autonomous roles in the core mesodermal cells.

Genes acting downstream of *Tbx1* in the core mesoderm

In addition to *Tcf21*, *Msc*, *Myf5* and *MyoD*, several interesting genes were altered when *Tbx1* was inactivated that might also explain resulting phenotypes. We identified two newly recognized core mesodermal genes, *Chrdl1* and *Lrrn1*, which were reduced in expression in $Tbx1^{-/-}$ embryos. Both are interesting genes that have not been studied with respect to formation of the muscles of mastication. The *Chrdl1* gene encodes a Bmp antagonist that has many different developmental functions. The human *CHRDL1* gene maps to the X chromosome. Recently, mutations in *CHRDL1* have been identified in humans causing X-linked megalocornea (MGC1; MIM#309300) (42). This is consistent with its expression pattern in the developing eye (43). There is not a mouse knockout allele available for *Chrdl1* to further analyze the craniofacial muscles. However,

craniofacial muscle defects have not been reported in humans with inactivating mutations. It is possible, based upon the human patient studies that *Chrdl1* may not be essential because other genes serve redundant functions. *Chordin* (*Chrd*) encodes another member of the gene family, but it is not expressed in the core mesodermal tissue, implicating other Bmp antagonists as possibly serving redundant functions. The *Grem1* gene encodes a Bmp antagonist and we found by microarray and qRT–PCR that it was reduced in expression in $Tbx1^{-/-}$ embryos. Inactivation of *Grem1* causes embryonic lethality with kidney and skeletal defects (44). *Grem1* is also important for regulating myogenic progenitor cell proliferation in skeletal muscle (45). The gene was weakly expressed in the mesoderm of PA1 in $Tbx1^{+/+}$ as well as $Tbx1^{-/-}$ embryos (21), suggesting that it may not be greatly affected by the *Tbx1* mutation. More work would need to be performed to understand the function of *Chrdl1*, *Grem1* and other Bmp antagonists downstream of *Tbx1*.

Lrrn1, encoding a transmembrane protein, was reduced in expression at E9.5 in $Tbx1^{-/-}$ embryos. It has a specific expression pattern in the telencephalon, core mesoderm and somites. Despite its intriguing expression pattern, $Lrrn1^{-/-}$ mice survive to adulthood (46). This would indicate that it is not essential for craniofacial muscle development. As for *Chrdl1*, *Lrrn1* might act redundantly with another gene(s). Relevant to this, there are three *Lrrn* family members in the mouse genome: *Lrrn1*, *Lrrn2* and *Lrrn3* (25), indicating that *Lrrn2* or *Lrrn3* might act redundantly. Chick *Lrrn2* is expressed in the second pharyngeal arch (PA2) core mesoderm but not PA1 (47). Neither *Lrrn2* nor *Lrrn3* is expressed in PA1 in mouse embryos at similar stages (25). Other more distant family members exist, sharing leucine-rich repeats (LRRs) and immunoglobulin-like (Ig) domains (48), suggesting that perhaps some of these might act redundantly with *Lrrn1*.

The two additional genes of interest that were identified are *Tcf12* and *Ash2l*. Both proteins TCF12 and ASH2L separately interact physically with myogenic regulatory factors, such as TCF21. The TCF12 protein, like the myogenic regulatory factors, is a bHLH E-box class of transcription factors, and as such can heterodimerize. Specifically, TCF21 can physically interact with TCF12 (49) implicating a possible molecular interaction. *Ash2l* (absent, small or homeotic-like, *Drosophila*) encodes a transcription regulator with histone methyltransferase activity. MYF5 and ASH2L are present in a shared protein–protein complex within cultured primary mouse myoblasts (50). Of interest, ASH2L physically interacts with TBX1 as identified using a yeast two hybrid screen (51). This suggests a possible molecular connection between ASH2L, TBX1 and MYF5 proteins. Another chromatin modifier, SETD7 (SET domain containing lysine methyltransferase 7), physically interacts with MYOD for myoblast differentiation (52) and separately interacts with TBX1 (53). *Ash21* and *Setd7* genes identified as part of the *Tbx1* gene network in PA1 were not changed in mRNA expression in $Tbx1^{-/-}$ embryos at E9.5 (Fig. 2B), but we may speculate that there are posttranslational modifications that alter protein–protein interactions.

One reason for loss of craniofacial muscle gene expression could be due to a change in cell fate, such as the cardiac lineage. This is because we found ectopic expression of cardiac morphogenetic genes, such as *GATA4*, *GATA5*, *GATA6* and *Tbx5*. However, these genes are not expressed in the core mesoderm, but are expressed in the caudal part of PA1 in $Tbx1^{-/-}$ embryos. The data are more consistent with loss of the core mesodermal lineage, as determined by fate mapping studies and apoptosis assays. Once precursors undergo apoptosis, the branchiomeric muscles can no longer form.

Genes downstream of *Tbx1* for pharyngeal development

There are other functions of *Tbx1* in craniofacial development besides forming the branchiomeric muscles. One important function is to control formation of the aortic arch arteries and their remodeling to form the asymmetric aortic arch. *Tbx1* is required for development and remodeling of the aortic arch arteries and mutant mice have similar defects as seen in 22q11DS patients (19,36,54). *Tbx1* was recently shown to act upstream of the *Gbx2* homeodomain transcription factor gene in the pharyngeal ectoderm and *Gbx2* acts upstream of Slit and Robo signaling in the neural crest cells for development of pharyngeal arch arteries 3, 4 and 6 (54). We found that *Gbx2*, *Robo1* and *Slit1* were reduced in expression in PA1 at E9.5 and/or E10.5, suggesting possible defects in PA1 artery formation.

There are other genes important for vascular development reduced in expression in $Tbx1^{-/-}$ embryos. The *Foxc1* and *Foxc2* as well as *Cxcl12* genes were reduced in expression in PA1 at E9.5 and/or E10.5. The two Forkhead transcription factor genes act redundantly upstream of CXCL12 ligand and its receptor CXCR4, and these proteins are required for chemotaxic motility of endothelial cells to form blood vessels (55). We observed a change in pattern of *Foxc1* expression and diminished *Foxc2* expression in the PA1 tissue in $Tbx1^{-/-}$ embryos at E10.5 coincident with microarray results. Neural crest cells do migrate into PA1 as determined by lineage tracing using *Wnt1-Cre* and a *ROSA26-LacZ* reporter gene in $Tbx1^{-/-}$ embryos and appear to be grossly normal (28). This work suggests that there is a change in cell fate rather than loss of tissue.

These genes may have roles in addition to that of vascular development. Specifically, knockout of *Foxc2* in the mouse results in cleft palate along with malformed mandible, skull bones and absent middle ear bones, similar to what is observed in $Tbx1^{-/-}$ embryos (31). Related to this, *Sim2* was reduced in expression in $Tbx1^{-/-}$ embryos at E10.5. *Sim2* encodes a transcription factor expressed in neural crest mesenchymal cells required for forming bones of the craniofacial region, including the palate (32). Based upon the *in situ* hybridization experiments presented in this report, we cannot rule out partial expression of *Sim2* in non-neural crest mesoderm; however, there are no obvious craniofacial muscle defects in $Sim2^{-/-}$ embryos (31). It is possible that altered *Foxc2* and *Sim2* expression in PA1 in $Tbx1^{-/-}$ embryos could contribute to the presence of a cleft palate and other craniofacial bone defects in later staged $Tbx1^{-/-}$ embryos. Similarly, changes in expression of these genes might help understand the basis of defects in the proximal mandible in PA1 in $Tbx1^{-/-}$ embryos (28). We previously found that *Fgf8* and *Bmp4* expression in the PA1 ectoderm at E10.5, as well as some downstream effector genes, was shifted laterally. We did not detect significant changes in gene expression levels of *Fgf8* and *Bmp4* (28). Additional genes that were reduced in expression that are expressed in neural crest mesenchymal cells but not yet linked to *Tbx1* are *Sox10*, *Six1* or *Six2* (56–58). It

is possible that change in *Fgf8* and *Bmp4* expression patterns could be a cause or effect of changes in expression pattern of these genes.

Hypoxic stress in PA1 of *Tbx1*$^{-/-}$ embryos

The mechanism by which loss of *Tbx1* results in increased apoptosis is not known. Some clues for this are derived from gene profiling at E10.5, where we found increased expression of hypoxic stress response genes. One trivial possibility for this increase is that PA1 cells undergo hypoxic stress secondary to vascular problems when *Tbx1* is inactivated (36,54). *Tbx1* is expressed early in development, before E8.5, but yet apoptosis does not take place until E9.5-E10.0. Similarly, many stress response genes were increased in expression by E10.5 but not at E9.5. This suggests that *Tbx1* may act with other genes to promote cell survival and stress in surrounding cells at these critical stages. Further studies of novel and known genes altered in expression or function between E9.5 and E10.5 should shed light on the relative hierarchy of stress response genes downstream of *Tbx1*.

SUMMARY

Our work demonstrates a key function of *Tbx1* in the core mesoderm itself for maintenance of cells and when inactivated, results in loss of muscles of mastication. We developed a gene network in which genes responsible for mesenchymal cell differentiation were highlighted as those reduced in expression or downregulated in the absence of *Tbx1*. We found that genes for cell stress are increased by E10.5 at a time period when the core mesoderm cells have undergone apoptosis. This sets the stage for future studies to identify direct transcriptional target genes and fully elucidate its role in myogenesis and or cell survival.

MATERIALS AND METHODS

Mouse mutants

The following mouse mutant alleles used in this study have been described previously: *Tbx1*$^{+/-}$ (20), *RCE*$^{EGFP/+}$ (59), *Tbx1*$^{flox/+}$ (39), *Tbx1*$^{Cre/+}$ (60), (*Mesp1*$^{Cre/+}$ (61) and *T-Cre* (62). *Tbx1*$^{+/-}$ mice, used to obtain *Tbx1*$^{-/-}$ embryos, have been maintained congenic in the Swiss Webster background. To generate *T-Cre*; *Mesp1*$^{Cre/+}$; *Tbx1*$^{flox/-}$ embryos, *T-Cre* transgenic mice were crossed to *Tbx1*$^{+/-}$ mice, on a mixed Swiss Webster background, to obtain *T-Cre*; *Tbx1*$^{+/-}$ mice, and these were then crossed with *Mesp1*$^{Cre/+}$mice to generate *T-Cre*; *Mesp1*$^{Cre/+}$; *Tbx1*$^{+/-}$ mice. These mice were then further crossed with the *Tbx1*$^{flox/flox}$ mice in a Swiss Webster background. Wild-type and *T-Cre*; *Mesp1*$^{Cre/+}$; *Tbx1*$^{flox/+}$ littermates were used as controls in relevant experiments. All other mouse strains used were maintained in a mixed Swiss Webster background. PCR strategies for mouse genotyping have been described in the original reports.

Histology

Mouse embryos were isolated in phosphate-buffered saline (PBS) and fixed in 10% neutral buffered formalin (Sigma) overnight. Following fixation, the embryos were dehydrated through a graded ethanol series, embedded in paraffin and sectioned at 5 μm. All sections were stained with hematoxylin and eosin using standard protocols. Some of the work was performed in the Einstein Histopathology Core Facility (http://www.einstein.yu.edu/histopathology/page.aspx).

RNA *in situ* hybridization

Whole-mount and tissue section RNA *in situ* hybridization with non-radioactive probes was performed as previously described (63,64), using PCR-based probes (Supplementary Material, Table S3).

Gene profiling

To obtain enough RNA for microarray hybridization experiments, dissected mandibular arches from three *Tbx1*$^{+/+}$ and three *Tbx1*$^{-/-}$ E9.5 and E10.5 embryos were pooled according to genotype, with three microarrays performed at each stage, in total. The tissue was homogenized in Buffer RLT (QIAGEN). Total RNA was isolated with the RNeasy Micro Kit according to the manufacturer's protocol. Quality and quantity of total RNA were determined using an Agilent 2100 Bioanalyzer (Agilent) and an ND-1000 Spectrophotometer (NanoDrop), respectively. Biotinylated single-stranded cDNA targets were amplified from 100 ng (ng) starting total RNA using the Ovation RNA Amplification System V2 and FL-Ovation cDNA Biotin Module V2 (NuGEN). A total of 3.75 μg of cDNA from the last step was hybridized to the GeneChip Test3 array (Affymetrix) to test the quality of the labeled target. Nucleic acid samples that passed quality control were then hybridized to the Affymetrix Mouse GeneST 1.0 (E9.5) or Affymetrix GeneChip Mouse Genome 430 2.0 Arrays (E10.5). Hybridization, washing, staining and scanning were performed in the Genomics Core at Einstein (http://www.einstein.yu.edu/genetics/CoreFacilities.aspx?id=23934) according to the Affymetrix manual. The microarray data have been uploaded to the GEO database (GSE30980 GSE35013).

Microarray statistical analysis for Affymetrix mouse gene ST arrays

GeneChip data were analyzed with oligo and limma (Linear Models for Microarray Analysis), which are two libraries present in the R package. Briefly, the original Affymetrix GeneChip CEL files generated by the Genomics Core were imported and summarized at the probe set level or at the transcript cluster level using the oligonucleotide library. Robust multi-array average (RMA) method was used to normalize, background correct and summarize. The data were converted to logarithmic scale and the significance analysis was performed using the two-sample *t*-test with a cut-off of unadjusted *P*-value of <0.05. The statistical analysis was performed using the Limma package.

Pathway and network analysis

Genes with a nominal *P*-value of <0.05 and a fold change of ≥ 1.3 were considered to be differently expressed and used to find associated and enriched biological processes and network

pathways using IPA and Genemania (http://www.ncbi.nlm.nih.gov/pubmed/20576703) for gene pathway groups shown in Figs 2C and 5.

Quantitative reverse transcriptase–polymerase chain reaction

To obtain enough total RNA and minimize the variability of gene expression in individual embryos, each tube contained microdissected PA1s at E10.5 from four embryos. Total RNA was isolated from dissected tissues from three independent biological replicates using the RNeasy Micro Kit (Qiagen) and analyzed for sample purity and integrity using BioAnalyzer instrumentation. The mRNA levels were measured by TaqMan Gene Expression Assays (Applied Biosystems) for each gene and were carried out in triplicate using *Ipo8* for the E9.5 and *Gapdh* for the E10.5 studies as normalization controls. TaqMan probes and primer sets were obtained from the Applied Biosystems' Gene Expression Assay database (http://allgenes.com). Samples were run in 96-well plates (10 μl final volume per reaction) on an ABI 7900HT Q-PCR apparatus. The sodium dodecyl sulfate 2.2 software platform (Applied Biosystems) was used for the computer interface with the ABI 7900HT PCR System to generate normalized data, compare samples and calculate the relative quantity. Statistical significance of the difference in gene expression was estimated using the two-tailed *t*-test.

Proliferation and apoptosis on tissue sections

After fixation as described for whole-mount direct fluorescence and embryo freezing, frozen sections were obtained at a thickness of 10 μm and then permeabilized in 0.5% Triton X-100 for 5 min. Blocking was performed with 5% serum (goat or donkey) in PBS/0.1% Triton X-100 (PBT) for 1 h. Primary antibody was diluted in blocking solution (1:500) and incubated for 1 h. Proliferation of cells was assessed by immunofluorescence using the primary antibody anti-phospho Histone H3 (Ser10), a mitosis marker (06–570 Millipore). Sections were washed in PBT and incubated with secondary antibody for 1 h. Secondary antibody was Alexa Fluor 568 goat α-rabbit IgG (A11011 Invitrogen) at 1:500. Slides were mounted in hard-set mounting medium with DAPI (Vector Labs H-1500). Images were captured using a Zeiss Axio Observer microscope. To perform statistical analysis of cell proliferation, we first calculated the average cell counts per tissue section for each embryo. Then, we estimated the mean and standard error of the average cell counts for control and mutant groups and compared them using the *t*-test. Apoptosis was assessed on frozen 10 μm thick sections by using DeadEnd Fluorometric TUNEL System (G3250 Promega) following the manufacturer's instructions. Natural GFP from the reporter or antibodies to GFP was used to distinguish the core mesodermal cells in both assays described above.

SUPPLEMENTARY MATERIAL

Supplementary Material is available at *HMG* online.

ACKNOWLEDGEMENTS

We thank the Department of Surgery at Montefiore Medical Center for providing salary support for Dr Carpenter. We thank Dr Antonio Baldini for the *Tbx1*^{Cre} mice. We thank Dr Mark Lewandoski for the *T-Cre* mice. We thank Nousin Haque and Harpreet Singh for their technical help. We acknowledge the Einstein Histopathology Core for embedding embryos and the Genomics Core for performing the gene expression profiling.

Conflict of Interest statement. None declared.

FUNDING

This work was supported by grants from the National Institutes of Health (R01HL088698 and P01HD070454, B.E.M.).

REFERENCES

1. Bryson-Richardson, R.J. and Currie, P.D. (2008) The genetics of vertebrate myogenesis. *Nat. Rev. Genet.*, **9**, 632–646.
2. Shprintzen, R.J. (2008) Velo-cardio-facial syndrome: 30 years of study. *Dev. Dis. Res. Rev.*, **14**, 3–10.
3. Shprintzen, R.J. and Marrinan, E. (2009) Velopharyngeal insufficiency: diagnosis and management. *Curr. Opin. Otolaryngol. Head Neck Surg.*, **17**, 302–307.
4. Zim, S., Schelper, R., Kellman, R., Tatum, S., Ploutz-Snyder, R. and Shprintzen, R. (2003) Thickness and histologic and histochemical properties of the superior pharyngeal constrictor muscle in velocardiofacial syndrome. *Arch. Facial Plast. Surg.*, **5**, 503–510.
5. Lypka, M., Bidros, R., Rizvi, M., Gaon, M., Rubenstein, A., Fox, D. and Cronin, E. (2010) Posterior pharyngeal augmentation in the treatment of velopharyngeal insufficiency: a 40-year experience. *Ann. Plast. Surg.*, **65**, 48–51.
6. Akcakus, M., Ozkul, Y., Gunes, T., Kurtoglu, S., Cetin, N., Kisaarslan, A.P. and Dundar, M. (2003) Associated anomalies in asymmetric crying facies and 22q11 deletion. *Genet. Couns.*, **14**, 325–330.
7. Noden, D.M. (1983) The embryonic origins of avian cephalic and cervical muscles and associated connective tissues. *Am. J. Anat.*, **168**, 257–276.
8. Trainor, P.A., Tan, S.S. and Tam, P.P. (1994) Cranial paraxial mesoderm: regionalisation of cell fate and impact on craniofacial development in mouse embryos. *Development*, **120**, 2397–2408.
9. Lu, J., Webb, R., Richardson, J.A. and Olson, E.N. (1999) MyoR: a muscle-restricted basic helix-loop-helix transcription factor that antagonizes the actions of MyoD. *Proc. Natl. Acad. Sci. USA.*, **96**, 552–557.
10. Moncaut, N., Cross, J.W., Siligan, C., Keith, A., Taylor, K., Rigby, P.W. and Carvajal, J.J. (2012) Musculin and TCF21 coordinate the maintenance of myogenic regulatory factor expression levels during mouse craniofacial development. *Development*, **139**, 958–967.
11. Semina, E.V., Reiter, R., Leysens, N.J., Alward, W.L., Small, K.W., Datson, N.A., Siegel-Bartelt, J., Bierke-Nelson, D., Bitoun, P., Zabel, B.U. *et al.* (1996) Cloning and characterization of a novel bicoid-related homeobox transcription factor gene, RIEG, involved in Rieger syndrome. *Nat. Genet.*, **14**, 392–399.
12. Kioussi, C., Briata, P., Baek, S.H., Wynshaw-Boris, A., Rose, D.W. and Rosenfeld, M.G. (2002) Pitx genes during cardiovascular development. *Cold Spring Harb. Symp. Quant. Biol.*, **67**, 81–87.
13. Ai, D., Liu, W., Ma, L., Dong, F., Lu, M.-F., Wang, D., Verzi, M.P., Cai, C., Gage, P.J., Evans, S. *et al.* (2006) Pitx2 regulates cardiac left-right asymmetry by patterning second cardiac lineage-derived myocardium. *Dev. Biol.*, **296**, 437–449.
14. Dong, F., Sun, X., Liu, W., Ai, D., Klysik, E., Lu, M.F., Hadley, J., Antoni, L., Chen, L., Baldini, A. *et al.* (2006) Pitx2 promotes development of splanchnic mesoderm-derived branchiomeric muscle. *Development*, **133**, 4891–4899.
15. Shih, H.P., Gross, M.K. and Kioussi, C. (2007) Cranial muscle defects of Pitx2 mutants result from specification defects in the first branchial arch. *Proc. Natl. Acad. Sci. USA.*, **104**, 5907–5912.

16. Nathan, E., Monovich, A., Tirosh-Finkel, L., Harrelson, Z., Rousso, T., Rinon, A., Harel, I., Evans, S.M. and Tzahor, E. (2008) The contribution of Islet1-expressing splanchnic mesoderm cells to distinct branchiomeric muscles reveals significant heterogeneity in head muscle development. *Development*, **135**, 647–657.
17. Harel, I., Maezawa, Y., Avraham, R., Rinon, A., Ma, H.Y., Cross, J.W., Leviatan, N., Hegesh, J., Roy, A., Jacob-Hirsch, J. *et al.* (2012) Pharyngeal mesoderm regulatory network controls cardiac and head muscle morphogenesis. *Proc. Natl. Acad. Sci. USA.*, **109**, 18839–18844.
18. Jerome, L.A. and Papaioannou, V.E. (2001) DiGeorge syndrome phenotype in mice mutant for the T-box gene, Tbx1. *Nat. Genet.*, **27**, 286–291.
19. Lindsay, E.A., Vitelli, F., Su, H., Morishima, M., Huynh, T., Pramparo, T., Jurecic, V., Ogunrinu, G., Sutherland, H.F., Scambler, P.J. *et al.* (2001) Tbx1 haploinsufficieny in the DiGeorge syndrome region causes aortic arch defects in mice. *Nature*, **410**, 97–9101.
20. Merscher, S., Funke, B., Epstein, J.A., Heyer, J., Puech, A., Lu, M.M., Xavier, R.J., Demay, M.B., Russell, R.G., Factor, S. *et al.* (2001) TBX1 is responsible for cardiovascular defects in velo-cardio-facial/DiGeorge syndrome. *Cell*, **104**, 619–629.
21. Kelly, R.G., Jerome-Majewska, L.A. and Papaioannou, V.E. (2004) The del22q11.2 candidate gene Tbx1 regulates branchiomeric myogenesis. *Hum. Mol. Genet.*, **13**, 2829–2840.
22. Grifone, R., Jarry, T., Dandonneau, M., Grenier, J., Duprez, D. and Kelly, R.G. (2008) Properties of branchiomeric and somite-derived muscle development in Tbx1 mutant embryos. *Dev. Dyn.*, **237**, 3071–3078.
23. Dastjerdi, A., Robson, L., Walker, R., Hadley, J., Zhang, Z., Rodriguez-Niedenfuhr, M., Ataliotis, P., Baldini, A., Scambler, P. and Francis-West, P. (2007) Tbx1 regulation of myogenic differentiation in the limb and cranial mesoderm. *Dev. Dyn.*, **236**, 353–363.
24. Liao, J., Kochilas, L., Nowotschin, S., Arnold, J.S., Aggarwal, V.S., Epstein, J.A., Brown, M.C., Adams, J. and Morrow, B.E. (2004) Full spectrum of malformations in velo-cardio-facial syndrome/DiGeorge syndrome mouse models by altering Tbx1 dosage. *Hum. Mol. Genet.*, **13**, 1577–1585.
25. Haines, B.P., Gupta, R., Jones, C.M., Summerbell, D. and Rigby, P.W. (2005) The NLRR gene family and mouse development: Modified differential display PCR identifies NLRR-1 as a gene expressed in early somitic myoblasts. *Dev. Biol.*, **281**, 145–159.
26. Seale, P., Ishibashi, J., Holterman, C. and Rudnicki, M.A. (2004) Muscle satellite cell-specific genes identified by genetic profiling of MyoD-deficient myogenic cell. *Dev. Biol.*, **275**, 287–300.
27. Coffinier, C., Tran, U., Larrain, J. and De Robertis, E.M. (2001) Neuralin-1 is a novel Chordin-related molecule expressed in the mouse neural plate. *Mech. Dev.*, **100**, 119–122.
28. Aggarwal, V.S., Carpenter, C., Freyer, L., Liao, J., Petti, M. and Morrow, B.E. (2010) Mesodermal Tbx1 is required for patterning the proximal mandible in mice. *Dev. Biol.*, **344**, 669–681.
29. Mussig, K., Staiger, H., Machicao, F., Thamer, C., Machann, J., Schick, F., Claussen, C.D., Stefan, N., Fritsche, A. and Haring, H.U. (2009) RARRES2, encoding the novel adipokine chemerin, is a genetic determinant of disproportionate regional body fat distribution: a comparative magnetic resonance imaging study. Metabolism, **58**, 519–524.
30. Aggarwal, V.S., Liao, J., Bondarev, A., Schimmang, T., Lewandoski, M., Locker, J., Shanske, A., Campione, M. and Morrow, B.E. (2006) Dissection of Tbx1 and Fgf interactions in mouse models of 22q11DS suggests functional redundancy. *Hum. Mol. Genet.*, **15**, 3219–3228.
31. Kume, T., Jiang, H., Topczewska, J.M. and Hogan, B.L. (2001) The murine winged helix transcription factors, Foxc1 and Foxc2, are both required for cardiovascular development and somitogenesis. *Genes Dev.*, **15**, 2470–2482.
32. Shamblott, M.J., Bugg, E.M., Lawler, A.M. and Gearhart, J.D. (2002) Craniofacial abnormalities resulting from targeted disruption of the murine Sim2 gene. *Dev. Dyn.*, **224**, 373–380.
33. Liao, J., Aggarwal, V.S., Nowotschin, S., Bondarev, A., Lipner, S. and Morrow, B.E. (2008) Identification of downstream genetic pathways of Tbx1 in the second heart field. *Dev. Biol.*, **316**, 524–537.
34. Ozawa, S., Ito, S., Kato, Y., Kubota, E. and Hata, R. (2010) Human p38 delta MAP kinase mediates UV irradiation induced up-regulation of the gene expression of chemokine BRAK/CXCL14. *Biochem. Biophys. Res. Commun.*, **396**, 1060–1064.
35. Shakib, K., Norman, J.T., Fine, L.G., Brown, L.R. and Godovac-Zimmermann, J. (2005) Proteomics profiling of nuclear proteins for kidney fibroblasts suggests hypoxia, meiosis, and cancer may meet in the nucleus. *Proteomics*, **5**, 2819–2838.
36. Zhang, Z., Cerrato, F., Xu, H., Vitelli, F., Morishima, M., Vincentz, J., Furuta, Y., Ma, L., Martin, J.F., Baldini, A. *et al.* (2005) Tbx1 expression in pharyngeal epithelia is necessary for pharyngeal arch artery development. *Development*, **132**, 5307–5315.
37. Balmer, J.E. and Blomhoff, R. (2002) Gene expression regulation by retinoic acid. *J. Lip. Res.*, **43**, 1773–1808.
38. Zhang, Z., Huynh, T. and Baldini, A. (2006) Mesodermal expression of Tbx1 is necessary and sufficient for pharyngeal arch and cardiac outflow tract development. *Development*, **133**, 3587–3595.
39. Arnold, J.S., Werling, U., Braunstein, E.M., Liao, J., Nowotschin, S., Edelmann, W., Hebert, J.M. and Morrow, B.E. (2006) Inactivation of Tbx1 in the pharyngeal endoderm results in 22q11DS malformations. *Development*, **133**, 977–987.
40. Sambasivan, R., Gayraud-Morel, B., Dumas, G., Cimper, C., Paisant, S., Kelly, R.G. and Tajbakhsh, S. (2009) Distinct regulatory cascades govern extraocular and pharyngeal arch muscle progenitor cell fates. *Dev. Cell*, **16**, 810–821.
41. Lu, J.R., Bassel-Duby, R., Hawkins, A., Chang, P., Valdez, R., Wu, H., Gan, L., Shelton, J.M., Richardson, J.A. and Olson, E.N. (2002) Control of facial muscle development by MyoR and capsulin. *Science*, **298**, 2378–2381.
42. Webb, T.R., Matarin, M., Gardner, J.C., Kelberman, D., Hassan, H., Ang, W., Michaelides, M., Ruddle, J.B., Pennell, C.E., Yazar, S. *et al.* (2012) X-linked megalocornea caused by mutations in CHRDL1 identifies an essential role for ventroptin in anterior segment development. *Am. J. Hum. Genet.*, **90**, 247–259.
43. Sakuta, H., Suzuki, R., Takahashi, H., Kato, A., Shintani, T., Iemura, S., Yamamoto, T.S., Ueno, N. and Noda, M. (2001) Ventroptin: a BMP-4 antagonist expressed in a double-gradient pattern in the retina. *Science*, **293**, 111–115.
44. Michos, O., Panman, L., Vintersten, K., Beier, K., Zeller, R. and Zuniga, A. (2004) Gremlin-mediated BMP antagonism induces the epithelial-mesenchymal feedback signaling controlling metanephric kidney and limb organogenesis. *Development*, **131**, 3401–3410.
45. Frank, N.Y., Kho, A.T., Schatton, T., Murphy, G.F., Molloy, M.J., Zhan, Q., Ramoni, M.F., Frank, M.H., Kohane, I.S. and Gussoni, E. (2006) Regulation of myogenic progenitor proliferation in human fetal skeletal muscle by BMP4 and its antagonist Gremlin. *J. Cell Biol.*, **175**, 99–110.
46. Tang, T., Li, L., Tang, J., Li, Y., Lin, W.Y., Martin, F., Grant, D., Solloway, M., Parker, L., Ye, W. *et al.* (2010) A mouse knockout library for secreted and transmembrane proteins. *Nat. Biotech.*, **28**, 749–755.
47. Andreae, L.C., Lumsden, A. and Gilthorpe, J.D. (2009) Chick Lrrn2, a novel downstream effector of Hoxb1 and Shh, functions in the selective targeting of rhombomere 4 motor neurons. *Neural Dev.*, **4**, 27.
48. Homma, S., Shimada, T., Hikake, T. and Yaginuma, H. (2009) Expression pattern of LRR and Ig domain-containing protein (LRRIG protein) in the early mouse embryo. *Gene Exp. Pattn.*, **9**, 1–26.
49. Tandon, P., Miteva, Y.V., Kuchenbrod, L.M., Cristea, I.M. and Conlon, F.L. (2013) Tcf21 regulates the specification and maturation of proepicardial cells. *Development*, **140**, 2409–2421.
50. McKinnell, I.W., Ishibashi, J., Le Grand, F., Punch, V.G., Addicks, G.C., Greenblatt, J.F., Dilworth, F.J. and Rudnicki, M.A. (2008) Pax7 activates myogenic genes by recruitment of a histone methyltransferase complex. *Nat. Cell Biol.*, **10**, 77–84.
51. Stoller, J.Z., Huang, L., Tan, C.C., Huang, F., Zhou, D.D., Yang, J., Gelb, B.D. and Epstein, J.A. (2010) Ash2l interacts with Tbx1 and is required during early embryogenesis. *Exp. Biol. Med. (Maywood)*, **235**, 569–576.
52. Tao, Y., Neppl, R.L., Huang, Z.P., Chen, J., Tang, R.H., Cao, R., Zhang, Y., Jin, S.W. and Wang, D.Z. (2011) The histone methyltransferase Set7/9 promotes myoblast differentiation and myofibril assembly. *J. Cell Biol.*, **194**, 551–565.
53. Chen, L., Fulcoli, F.G., Ferrentino, R., Martucciello, S., Illingworth, E.A. and Baldini, A. (2012) Transcriptional control in cardiac progenitors: Tbx1 interacts with the BAF chromatin remodeling complex and regulates Wnt5a. *PLoS Genet.*, **8**, e1002571.
54. Calmont, A., Ivins, S., Van Bueren, K.L., Papangeli, I., Kyriakopoulou, V., Andrews, W.D., Martin, J.F., Moon, A.M., Illingworth, E.A., Basson, M.A. *et al.* (2009) Tbx1 controls cardiac neural crest cell migration during arch artery development by regulating Gbx2 expression in the pharyngeal ectoderm. *Development*, **136**, 3173–3183.
55. Hayashi, H. and Kume, T. (2008) Forkhead transcription factors regulate expression of the chemokine receptor CXCR4 in endothelial cells and CXCL12-induced cell migration. *Biochem. Biophys. Res. Commun.*, **367**, 584–589.

56. Kutejova, E., Engist, B., Mallo, M., Kanzler, B. and Bobola, N. (2005) Hoxa2 downregulates Six2 in the neural crest-derived mesenchyme. *Development*, **132**, 469–478.
57. Gavalas, A., Trainor, P., Ariza-McNaughton, L. and Krumlauf, R. (2001) Synergy between Hoxa1 and Hoxb1: the relationship between arch patterning and the generation of cranial neural crest. *Development*, **128**, 3017–3027.
58. Oliver, G., Wehr, R., Jenkins, N.A., Copeland, N.G., Cheyette, B.N., Hartenstein, V., Zipursky, S.L. and Gruss, P. (1995) Homeobox genes and connective tissue patterning. *Development*, **121**, 693–705.
59. Sousa, V.H., Miyoshi, G., Hjerling-Leffler, J., Karayannis, T. and Fishell, G. (2009) Characterization of Nkx6–2-derived neocortical interneuron lineages. *Cere. Cortex*, **19**(Suppl 1), 1–10.
60. Vitelli, F., Huynh, T. and Baldini, A. (2009) Gain of function of Tbx1 affects pharyngeal and heart development in the mouse. *Genesis*, **47**, 188–195.
61. Saga, Y., Miyagawa-Tomita, S., Takagi, A., Kitajima, S., Miyazaki, J. and Inoue, T. (1999) MesP1 is expressed in the heart precursor cells and required for the formation of a single heart tube. *Development*, **126**, 3437–3447.
62. Perantoni, A.O., Timofeeva, O., Naillat, F., Richman, C., Pajni-Underwood, S., Wilson, C., Vainio, S., Dove, L.F. and Lewandoski, M. (2005) Inactivation of FGF8 in early mesoderm reveals an essential role in kidney development. *Development*, **132**, 3859–3871.
63. Hidai, H., Bardales, R., Goodwin, R., Quertermous, T. and Quertermous, E.E. (1998) Cloning of capsulin, a basic helix-loop-helix factor expressed in progenitor cells of the pericardium and the coronary arteries. *Mech. Dev.*, **73**, 33–43.
64. Alappat, S.R., Zhang, Z., Suzuki, K., Zhang, X., Liu, H., Jiang, R., Yamada, G. and Chen, Y. (2005) The cellular and molecular etiology of the cleft secondary palate in Fgf10 mutant mice. *Dev. Biol.*, **277**, 102–113.